

AD-A017 400

DAMAGE PROFILES IN SILICON AND THEIR IMPACT ON  
DEVICE RELIABILITY

G. H. Schwuttke

International Business Machines Corporation

Prepared for:

Advanced Research Projects Agency

1 July 1975

DISTRIBUTED BY:



National Technical Information Service  
U. S. DEPARTMENT OF COMMERCE

ADA017400

# DAMAGE PROFILES IN SILICON and THEIR IMPACT ON DEVICE RELIABILITY

328162

G. H. Schwuttke, Principal Investigator (914) 897-3140  
International Business Machines Corporation  
System Products Division, East Fishkill Laboratories  
Hopewell Junction, New York 12533

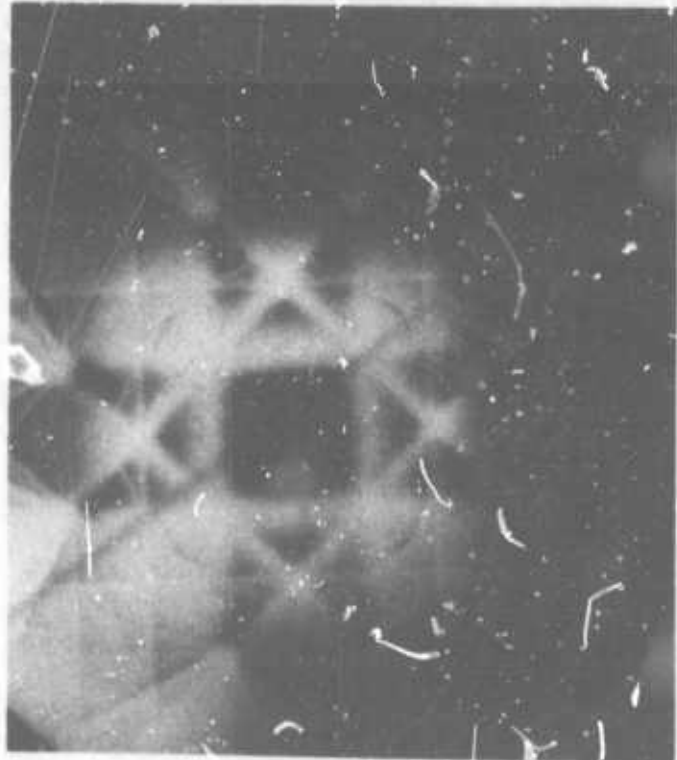
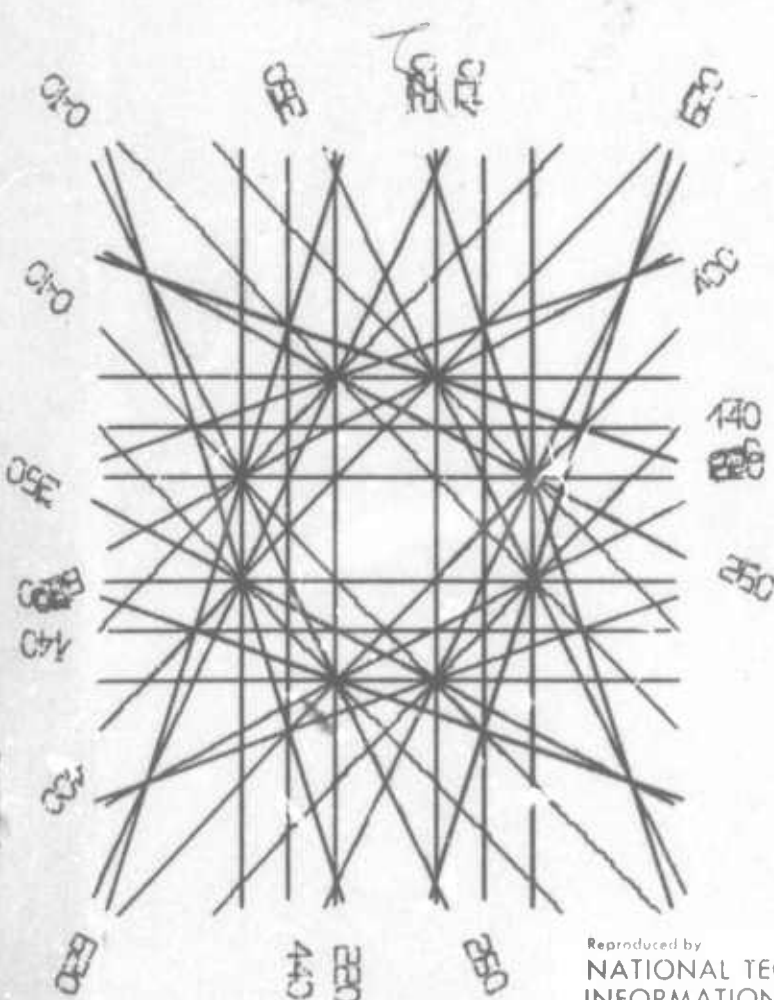
TECHNICAL REPORT No. 6  
July 1975

Contract No. DAHC15-72-C-0274  
Contract Monitor: Dr. C. M. Stickley

Sponsored by  
Advanced Research Projects Agency  
ARPA Order No. 2196, Program Code No. P2D10

DISTRIBUTION STATEMENT A

Approved for public release  
Distribution Unlimited



Reproduced by  
NATIONAL TECHNICAL  
INFORMATION SERVICE  
U.S. Department of Commerce  
Springfield, VA 22151

Kikuchi Map of (001) Silicon.  
(Left) Computer generated.  
(Right) Micrograph taken with  
200 keV electrons.

DD  
REF ID: A  
SEP 18 1975  
B  
65

Unclassified

Security Classification

DOCUMENT CONTROL DATA - R&D

(Security classification of title, body of abstract and indexing annotation must be entered when the overall report is classified)

1. ORIGINATING ACTIVITY (Corporate author) International Business Machines Corporation System Products Division, East Fishkill Hopewell Junction, N.Y. 12533	2a. REPORT SECURITY CLASSIFICATION Unclassified
2b. GROUP	

3. REPORT TITLE

DAMAGE PROFILES IN SILICON  
AND THEIR IMPACT ON DEVICE RELIABILITY

4. DESCRIPTIVE NOTES (Type of report and inclusive dates)

Scientific 1 January 1975 to 30 June 1975

5. AUTHOR(S) (First name, middle initial, last name)

G. H. Schwuttke

6. REPORT DATE 1 July 1975	7a. TOTAL NO. OF PAGES 65	7b. NO. OF REFS 23
8a. CONTRACT OR GRANT NO. DAHC 15-72-C-0274	9a. ORIGINATOR'S REPORT NUMBER(S) TR-22.1921	
b. PROJECT, TASK, WORK UNIT NOS.		
c. DOD ELEMENT	9b. OTHER REPORT NO(S) (Any other numbers that may be assigned this report)	
d. DOD SUBELEMENT		
10. DISTRIBUTION STATEMENT		
11. SUPPLEMENTARY NOTES		12. SPONSORING MILITARY ACTIVITY Advanced Research Projects Agency
13. ABSTRACT		

This report summarizes investigations done during the contract period of January 1, 1975, to June 30, 1975. It describes work dealing with improvements of advanced measurement techniques. Chapter 1 deals with the computer generation of Kikuchi patterns needed for complex structural analysis of crystal defects in silicon. The program is applicable to a large variety of problems and can be used to generate Kikuchi maps for different crystal structures, each desired crystal orientation, and electron energy. The program can also be used to generate channeling patterns for scanning electron microscopy application. The report provides a complete set of computer-generated Kikuchi maps for silicon and 200 keV electrons. A complete program in Fortran IV using an IBM 1800 computer is also given. The second part describes the application of MOS C-V and MOS G-V measurements for the evaluation of epitaxial films on silicon or insulator substrates. It is shown that the presence of an underlying junction requires important precautions with use of the MOS C-V measurement technique. The junction requires an increased number of components in the equivalent network, which impedes the analysis. This chapter shows how to solve the problem. Values for MOS dot diameter, layer and substrate resistivity, oxide thickness, etc. are given and refer to ranges where meaningful lifetime measurements can be carried out.

Unclassified

Security Classification

Unclassified

Security Classification

14. KEY WORDS	LINK A		LINK B		LINK C	
	ROLE	WT	HOLE	WT	ROLE	WT
Silicon Defect analysis Kikuchi patterns Transmission electron microscopy Epitaxial layers Lifetime measurements						

ia

Unclassified

Security Classification

CONTENTS	PAGE
List of Investigators	ii
Summary	iii
<b>Chapter 1</b>	
<b>Computer Generation of Kikuchi Maps for     Transmission Electron Microscopy (TEM) and     Scanning Electron Microscopy (SEM)     Investigations</b>	
by H. Kappert	
Introduction	1
Geometry	2
Orientation	6
The Program	17
Selection of Diffraction Planes	
Transition to Desired Orientation	
Rejection of High Index and High Order Planes	
Calculation of Coordinates	
Determination of Radius and Center of Kikuchi Circle	
Provision for an (x,y) Array for the Plot	
Plotting Section	
Plotting the Pole Map	
Results	21
References	24
Appendix: Program in Fortran IV for IBM 1800 Computer	25

## **Chapter 2**

### **Electrical Characterization of Quasi MOS Structures on Silicon**

**by W. R. Fahrner, E. F. Gorey, and C. P. Schneider**

<b>Introduction</b>	<b>38</b>
<b>Analysis of Equivalent Network</b>	<b>39</b>
<b>Spreading Resistance vs. Dot Diameter</b>	<b>48</b>
<b>Range of Quasi MOS Capacitance Technique</b>	<b>50</b>
<b>Comparison With Other Techniques</b>	<b>51</b>
<b>Results and Discussion</b>	<b>52</b>
<b>Summary and Conclusions</b>	<b>55</b>
<b>References</b>	<b>56</b>

### **LIST OF INVESTIGATORS**

The project is supervised by Dr. G. H. Schwuttke, principal investigator. The following people contributed to the work in this report:

<b>Dr. W. Fahrner</b>	- Investigator (Visiting Scientist)
<b>Dr. H. Kappert</b>	- Investigator (Visiting Scientist)
<b>Dr. G. H. Schwuttke</b>	- Principal Investigator
<b>Mr. E. F. Gorey</b>	- Technical Support
<b>Mr. C. P. Schneider</b>	- Technical Support
<b>Mr. H. Ilker</b>	- Technical Support

## SUMMARY

This report summarizes work done during the contract period of January 1, 1975 to June 30, 1975. It describes research programs dealing with improvements of advanced measurement techniques. Such improvements became imperative during the course of the contract work and are needed for subsequent structural and electrical characterization of impact sound stressed (ISS'ed) silicon wafers before and after oxidation and epitaxy.

The first chapter advances the analytical capabilities of transmission electron microscopy through the application of computer-generated Kikuchi patterns. Kikuchi lines in electron diffraction patterns are used for complex crystal defect analysis based on two-beam orientation of the specimen. Since our Hitachi microscope permits seeing only about  $4^\circ$  of a diffraction pattern it is impossible to index Kikuchi lines without a detailed Kikuchi map. Therefore it was necessary to computer-generate Kikuchi plots. A program for the generation of such plots was written. The program was used to generate Kikuchi maps for the three main orientations (001), (011) and (111) for Si and 200 keV electrons.

An additional benefit of this computer program is that it is applicable to a large variety of problems. By changing proper parameters the same program can be used to generate maps for all kinds of crystal structures, each desired crystal orientation, electron energy, crystallographic order and maximum index-number of lines. The program considers also parameters such as map-scales and camera length of the microscope.

In addition the program can be used to compute and print out channeling patterns used for crystal orientation analysis in the scanning electron microscope. The report provides a complete set of Kikuchi maps for silicon and 200 keV electrons as well as the complete program to generate other patterns.

The second part of the report describes the application of MOS C-V measurements to the evaluation of epitaxial silicon films on silicon or insulator substrates. It is shown that the presence of a semiconductor junction under the MOS structure requires certain considerations to be made if meaningful measurements are to be obtained. The junction requires an increased number of components in the equivalent network, which impedes the analysis.

A solution to this problem is given. If one side of the junction is oxidized, a quasi MOS structure is obtained. The equivalent network of such a structure is discussed and the conditions for MOS C-V and G-V measurements are given. When the MOS admittance can be measured the following information can be obtained:

1. Surface-state density, the corresponding capture cross sections, the charge density in the oxide, and deep energy levels.
2. The doping concentration.
3. The minority carrier lifetime.

The discussion concentrates on the measurement of minority carrier lifetime in epitaxial silicon films. Values for layer and substrate resistivity, dot diameter, oxide thickness, etc., are given to establish the range for this "Quasi MOS Capacitance Technique."

## **Chapter 1**

### **COMPUTER GENERATION OF KIKUCHI MAPS FOR TRANSMISSION ELECTRON MICROSCOPY (TEM) AND SCANNING ELECTRON MICROSCOPY (SEM) INVESTIGATIONS**

**by**

**H. Kappert**

#### **INTRODUCTION**

Electron diffraction patterns of samples of very good crystalline perfection and of a thickness such that inelastic scattering of electrons is fairly high, show a distinct line structure superimposed on the background intensity. This line pattern is known as the Kikuchi pattern. A similar pattern (known as Coates or channeling pattern) appears in the SEM when the intensity of the backscattered electrons is recorded as an angular dependence of the incoming beam in reference to the sample orientation.

Several applications of the TEM technique such as Burgers vector determination, crystal orientation determination, and indexing of unknown spot pattern make use of such Kikuchi patterns (1-8). For such applications it is convenient to have Kikuchi maps which show the geometrical configuration of the pattern and give the indices of all lines in it.

One way to obtain such maps is to take many images in the TEM of overlapping parts of the diffraction pattern for different tilt angles of the specimen and assemble these images in a composite map. Another way is to generate plots of indexed

Kikuchi maps through a computer. The advantage of the second way is that once a program is available it is very easy to select any desired crystalline structure, sample orientation, different wavelength of electrons or even x-rays, scale of map, or order of Kikuchi lines, just by changing some parameters in the program.

To generate Kikuchi maps very good instructions can be found in the literature (4,7,9). We followed mainly the recipe given by C. T. Young and J. L. Lytton (9).

#### GEOMETRY

Kikuchi lines are originated by inelastically scattered electrons in the specimen. The energy losses of these electrons are small enough that they still can be considered coherent, but they have changed direction in reference to the primary electron beam. Therefore, in spite of the primary beam being off Bragg angle  $\theta$  for a certain set of net planes, a particular fraction of the inelastically scattered electrons makes a Bragg reflection at these planes, e.g., (h, k, l) in Fig. 1. This can be regarded as a virtual incoming electron beam for each set of net planes, which is split below the specimen into a transmitted and a diffracted part. We find this situation not only in the plane that corresponds to the plane of the drawing in Fig. 1 but in all directions whenever the Bragg

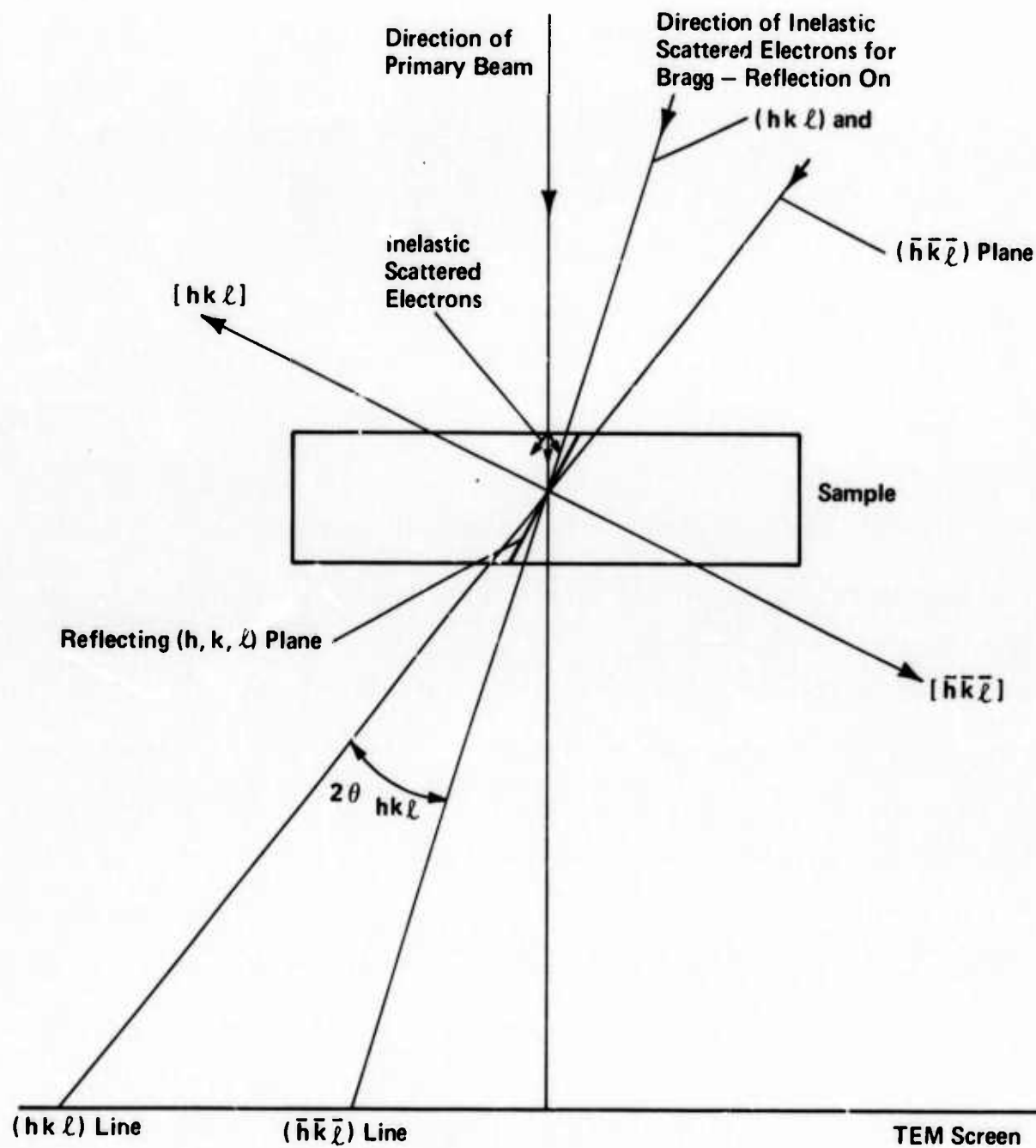


Fig. 1. Geometry for formation of Kikuchi lines.

condition is satisfied for the  $(h, k, l)$  plane. Therefore all the directions of the particular fraction of elastically scattered electrons in Bragg conditions for a certain set of net planes  $(h, k, l)$  are represented by a cone (Fig. 2), where the cone axis is in the direction of the plane normal  $(h, k, l)$  and the half opening angle is  $90^\circ - \theta$  (Kossel cone). The same geometry can be used for channeling patterns in the SEM. In the SFM the primary beam itself has to be tilted along a cone surface to get a signal of the backscattered electrons with less or more intensity than for the background intensity that appears as dark or bright lines on the TV display.

The real Kikuchi line pattern is the intersection of all the cones produced by the different sets of net planes, with the image plane in the TEM below the specimen. The real channeling pattern is the intensity modulation of the backscattered electrons above the sample, as seen by the collector and displayed on the TV screen, dependent on the tilt angle of the primary beam in reference to the sample orientation.

The usual way to generate Kikuchi and channeling maps is to make a stereographic projection of all the cones, which are thus represented as circles on the projection sphere (Fig. 2). This may be done because the projection keeps the angles between intersecting lines or circles on the sphere constant, results in only small distortions of the distances especially

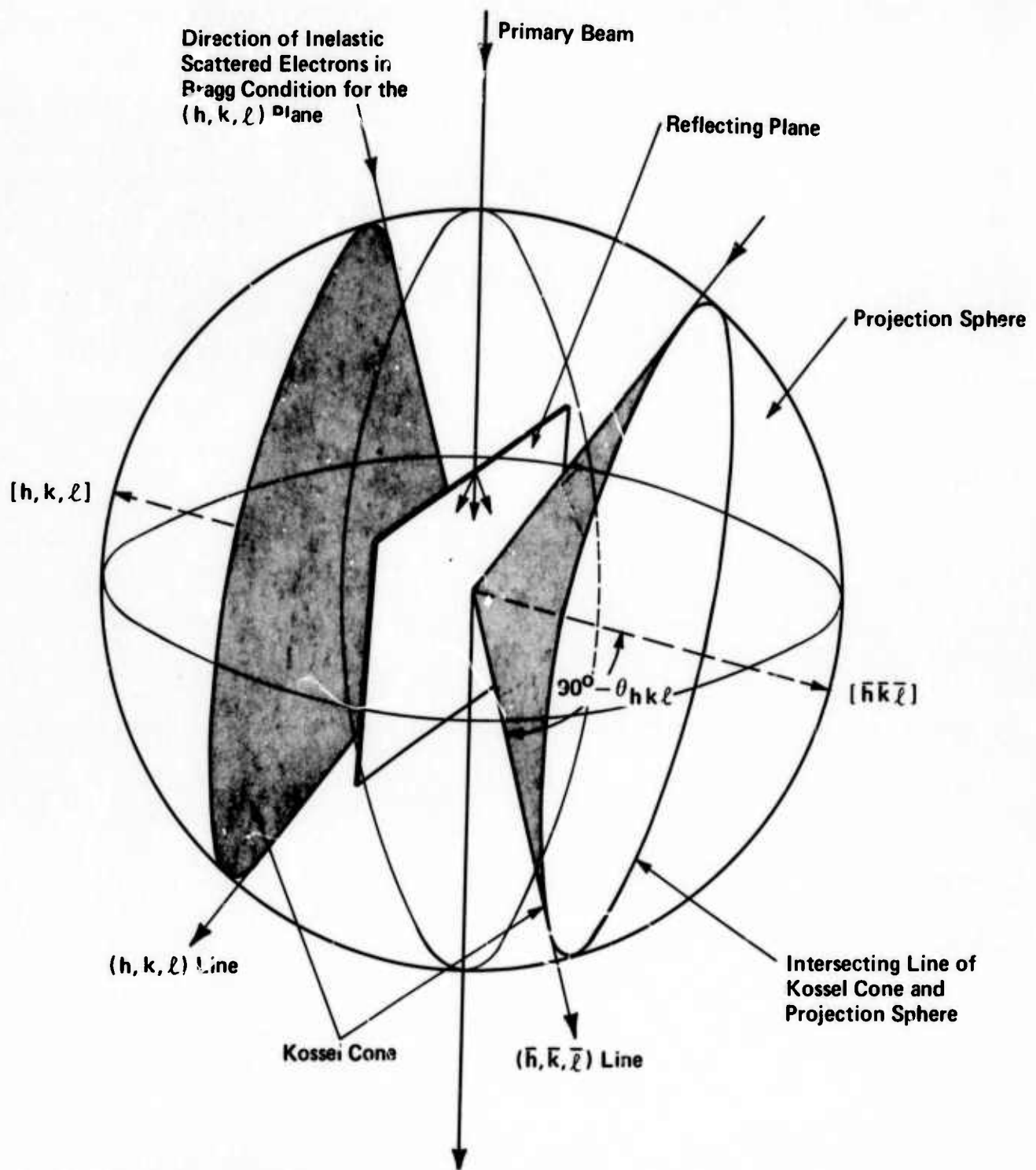


Fig. 2. Geometry of Kossel cones and their intersection with the projection sphere.

close to the center pole , and has the advantage that standard stereographic pole maps can be used for indexing purposes. The stereographic projection of the intersecting lines of the diffraction cones with the projection sphere appears as circles in the projection plane, which are called Kikuchi circles. The radius and center of each Kikuchi circle has to be calculated. Subsequently the part of the circle that is within the plotting area has to be determined and to be drawn.

#### ORIENTATION

Standard stereographic projections are made from G to O and are observed from the top, as shown in Fig. 3. The channeling patterns in the SEM are observed in the same way. To find the correct orientation between standard stereographic pole maps, channeling map and channeling pattern on the screen, we have only to consider which lenses are used to focus the primary beam onto the sample surface and how the tilt angle is related to the TV display.

The G to O direction of the standard stereographic projection, as shown in Fig. 3, is just the opposite to the direction in which the electrons go in the TEM to form the Kikuchi pattern on the screen. One gets around this orientation problem

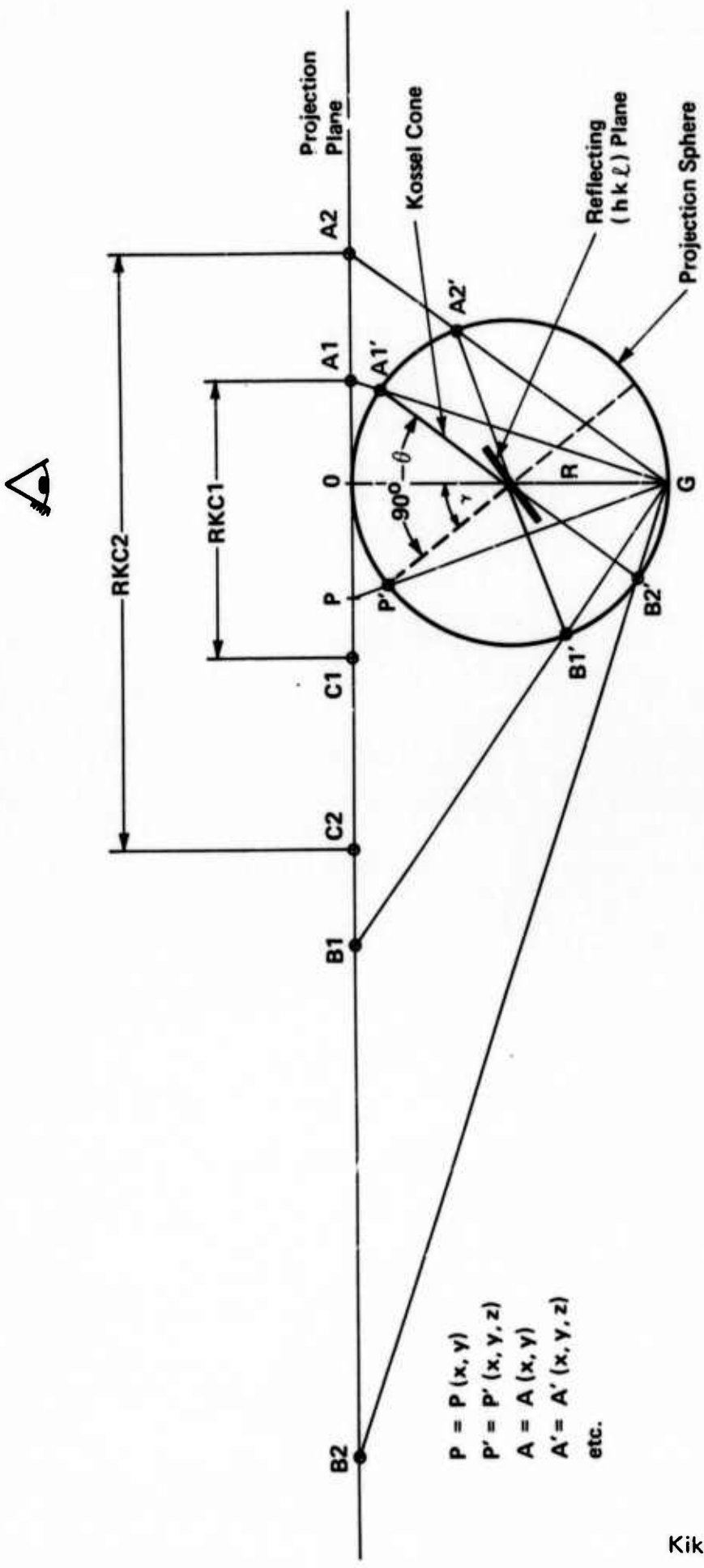


Fig. 3. Used projection and geometry to calculate radius and center of the Kikuchi circles.

by turning the projection upside down (1). Therefore standard stereographic projections have to be inverted for indexing purposes. Another possibility is to use the standard stereographic projection without inversion. This requires an adjustment of the Kikuchi maps such that the indexed reflections in the diffraction pattern correspond to the planes in the crystal. From the geometry shown in Fig. 2, one can see that the cone representing the directions of diffracted electrons intersects the projection sphere at the lower hemisphere as well as at the upper hemisphere. A downward projection--that is, the unconventional projection from O to G (Fig. 3)--would result in the real Kikuchi map as seen on the TEM screen.

An upward projection--that is, the conventional stereographic projection from G to O (Fig. 3)--results in the same map, except that this one is rotated by  $180^\circ$  in reference to the real Kikuchi pattern on the TEM screen. To do it this way was recently proposed by Head et al. (10). We decided to use this method because a rotation of  $180^\circ$  is more convenient than a mirror inversion, and we can use standard stereographic projections as in x-ray studies.

The correct orientation between the sample, the TEM micrograph, the diffraction pattern, standard pole map and Kikuchi map is found as follows:

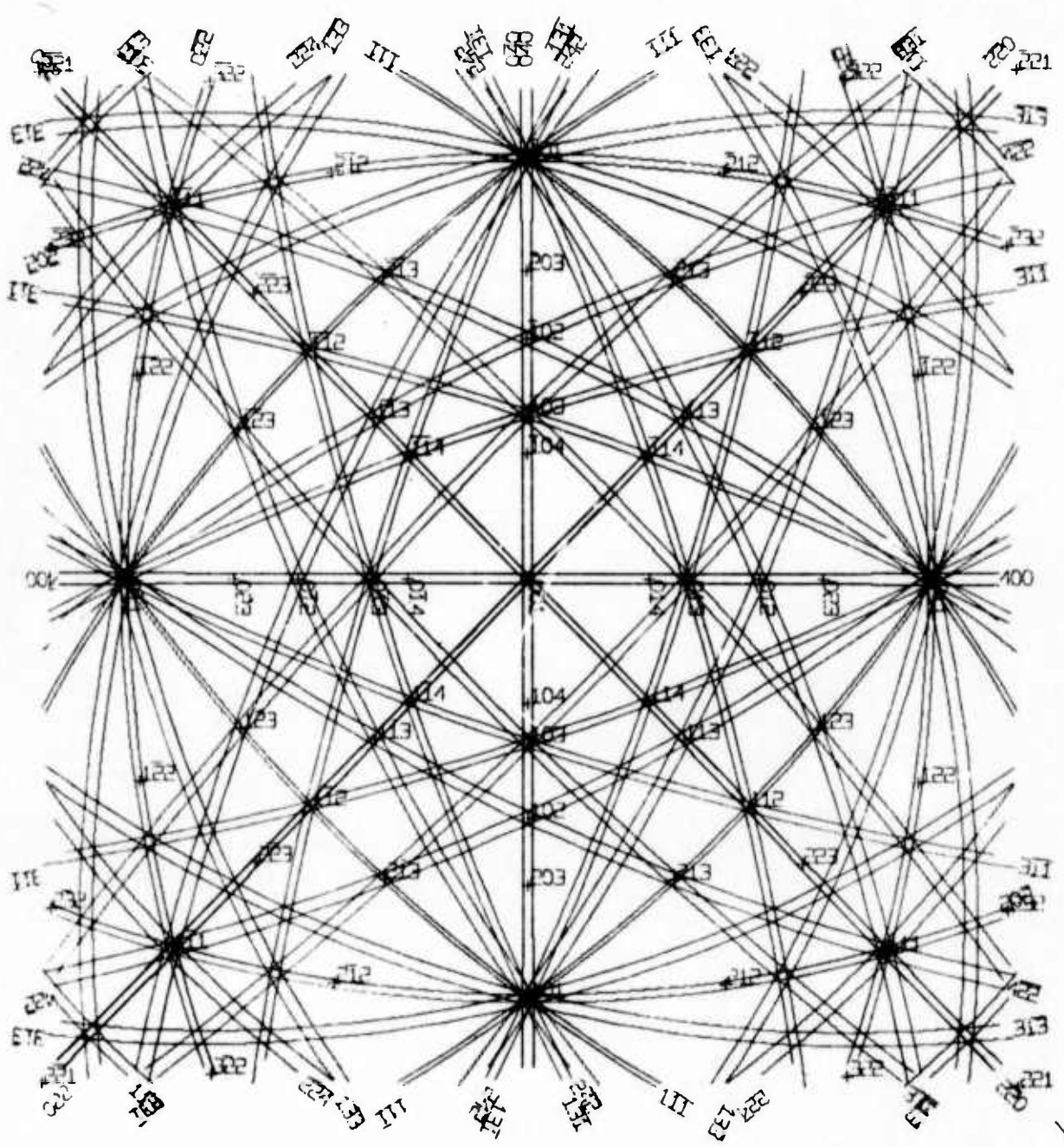
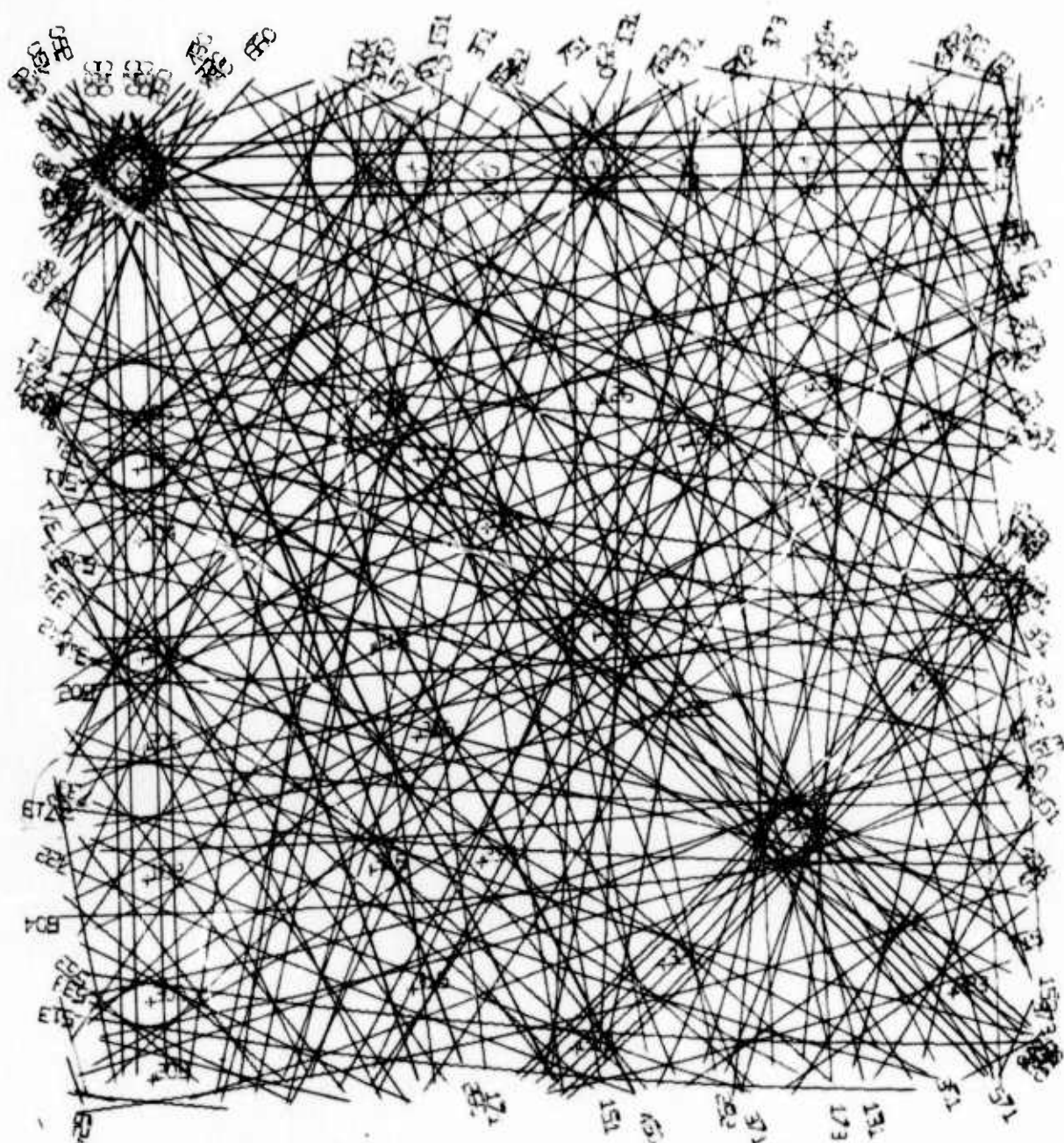


Fig. 4. (001) map for Si 200 keV,  $x_0 = y_0 = 11\text{cm}$ ,  $R = 11\text{cm}$ , RMN = 2, SMSQ = 5.



Reproduced from  
best available copy.

Fig. 5. (001) map for Si 200 keV,  $x_0 = y_0 = 20\text{cm}$ ,  $R = 32\text{cm}$ , RMN = 4, SMSQ = 9.

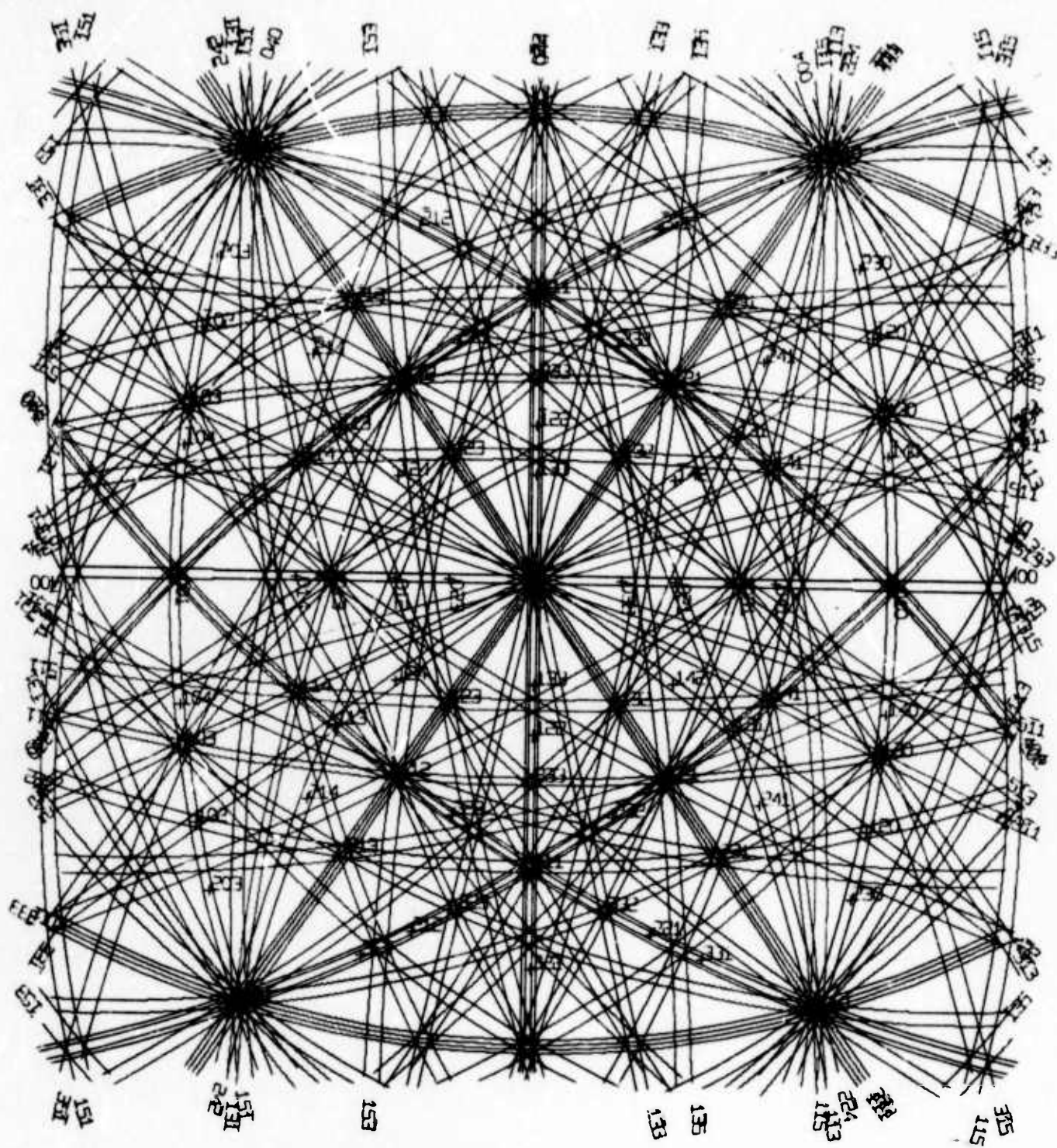


Fig. 6. (011) map for Si 200 keV,  $x_0 = y_0 = 12\text{cm}$ ,  $R = 11\text{cm}$ , RMN = 4, SMSQ = 5.

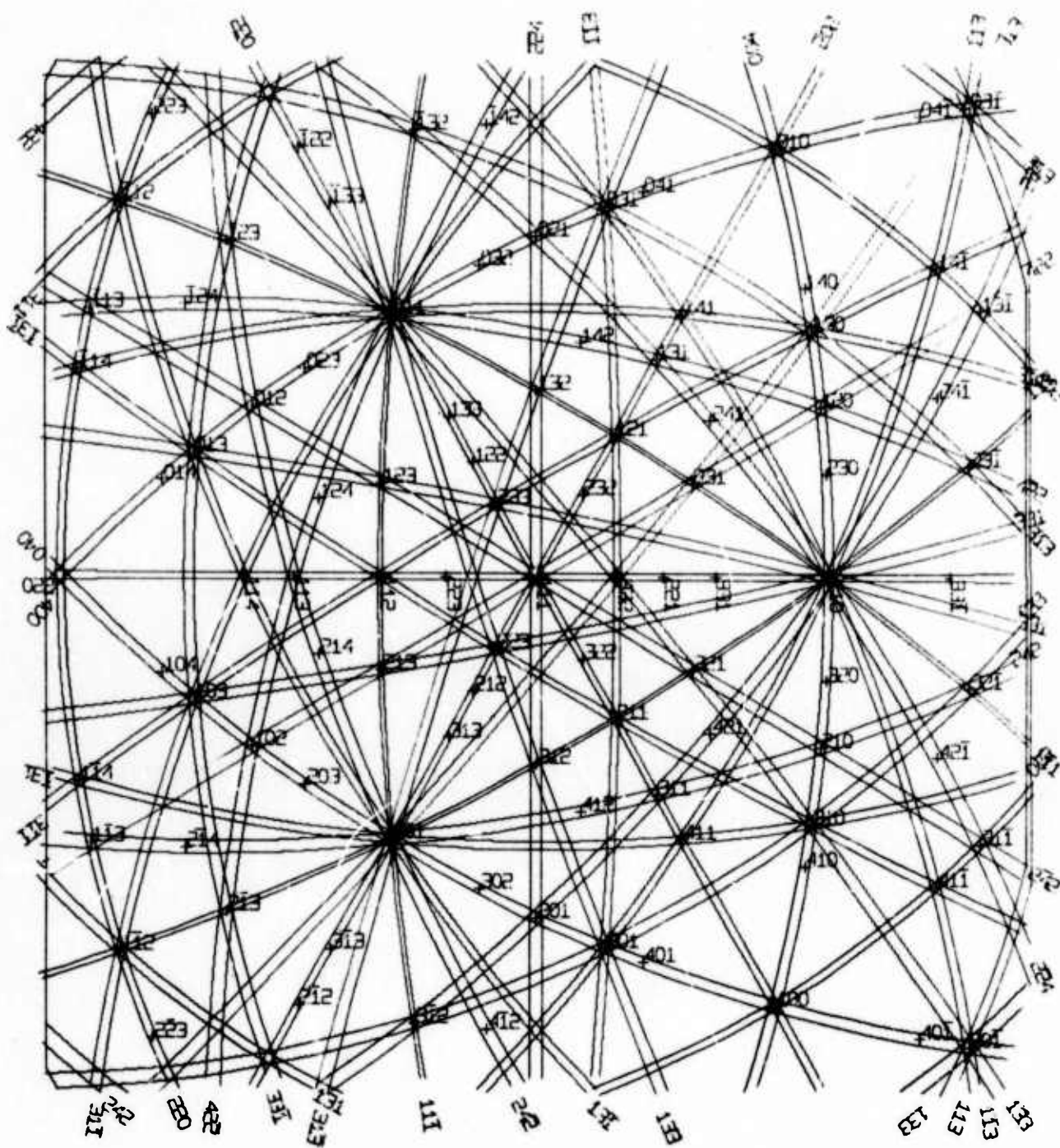
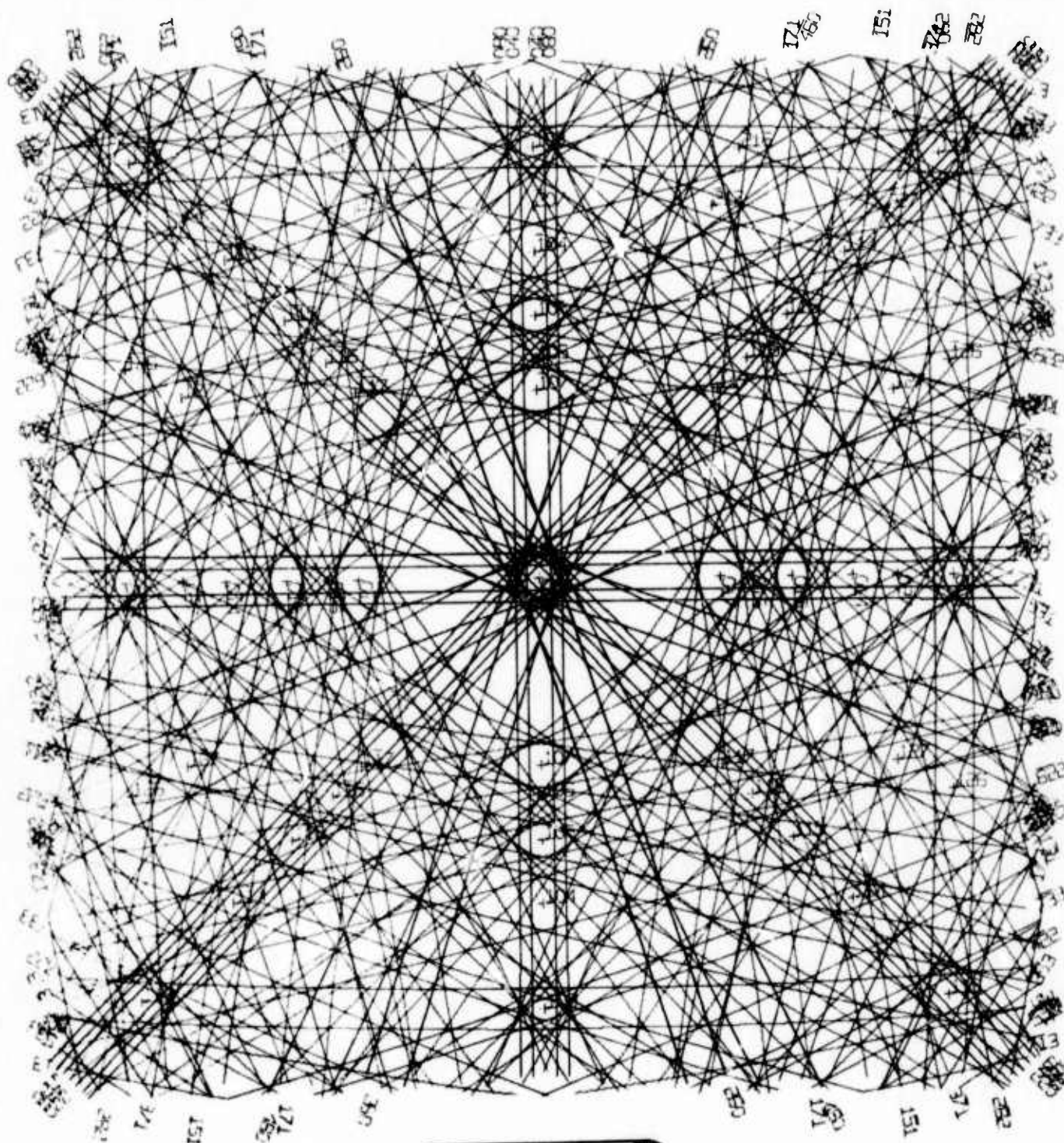


Fig. 7. (111) map for Si 200 keV,  $x_0 = y_0 = 12\text{cm}$ ,  $R = 11\text{cm}$ , RMN = 2, SMSQ = 5.



Reproduced from  
best available copy.

Fig. 8. (001) map for Si 200 keV,  $x_0 = y_0 = 12\text{cm}$ ,  $R = 32\text{cm}$ , RMN = 4, SMSQ = 9.

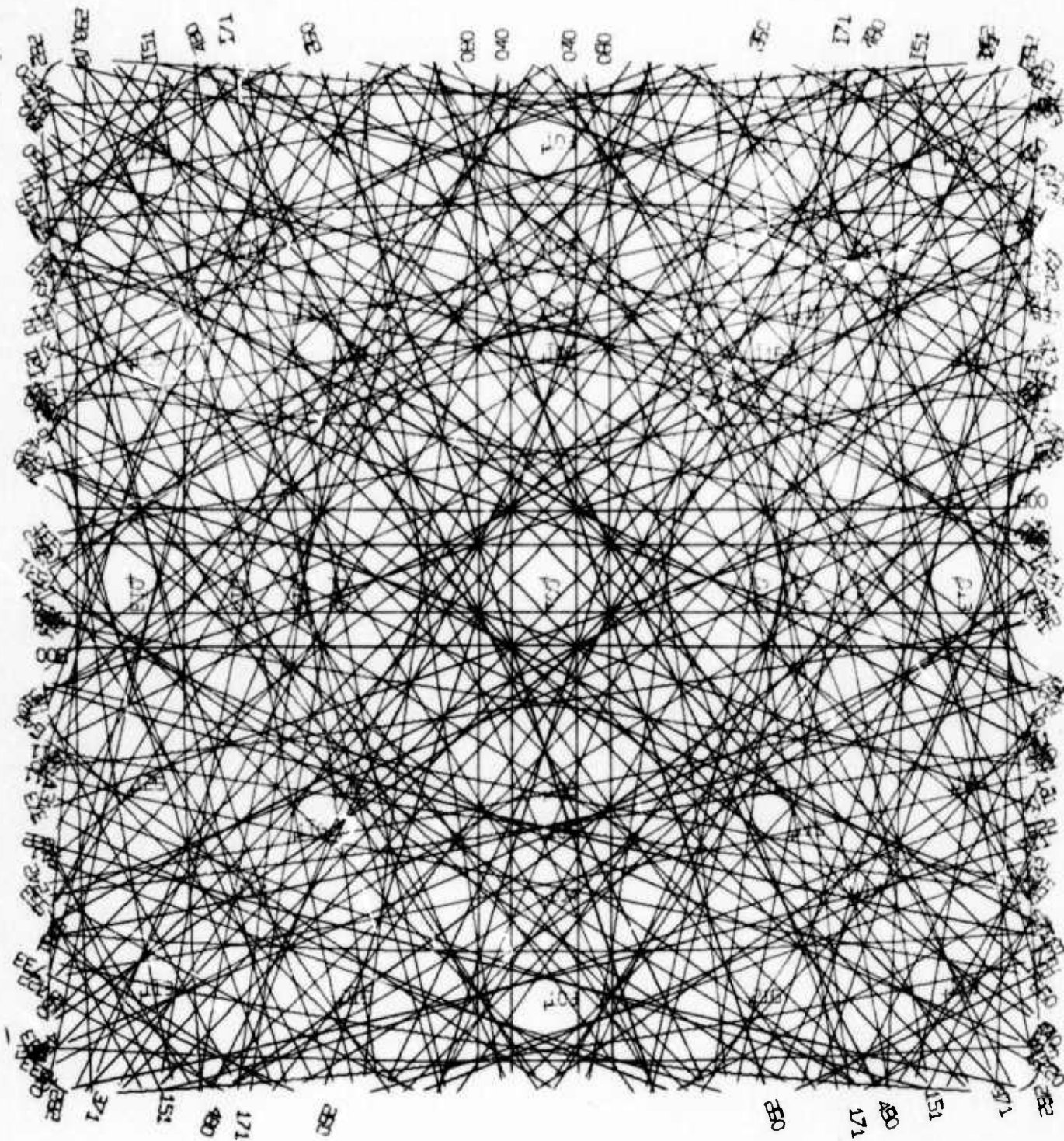


Fig. 9. (001) map for Si 30 keV,  $x_0 = y_0 = 12\text{cm}$ ,  $R = 32\text{cm}$ , RMN = 4, SMSQ = 9.

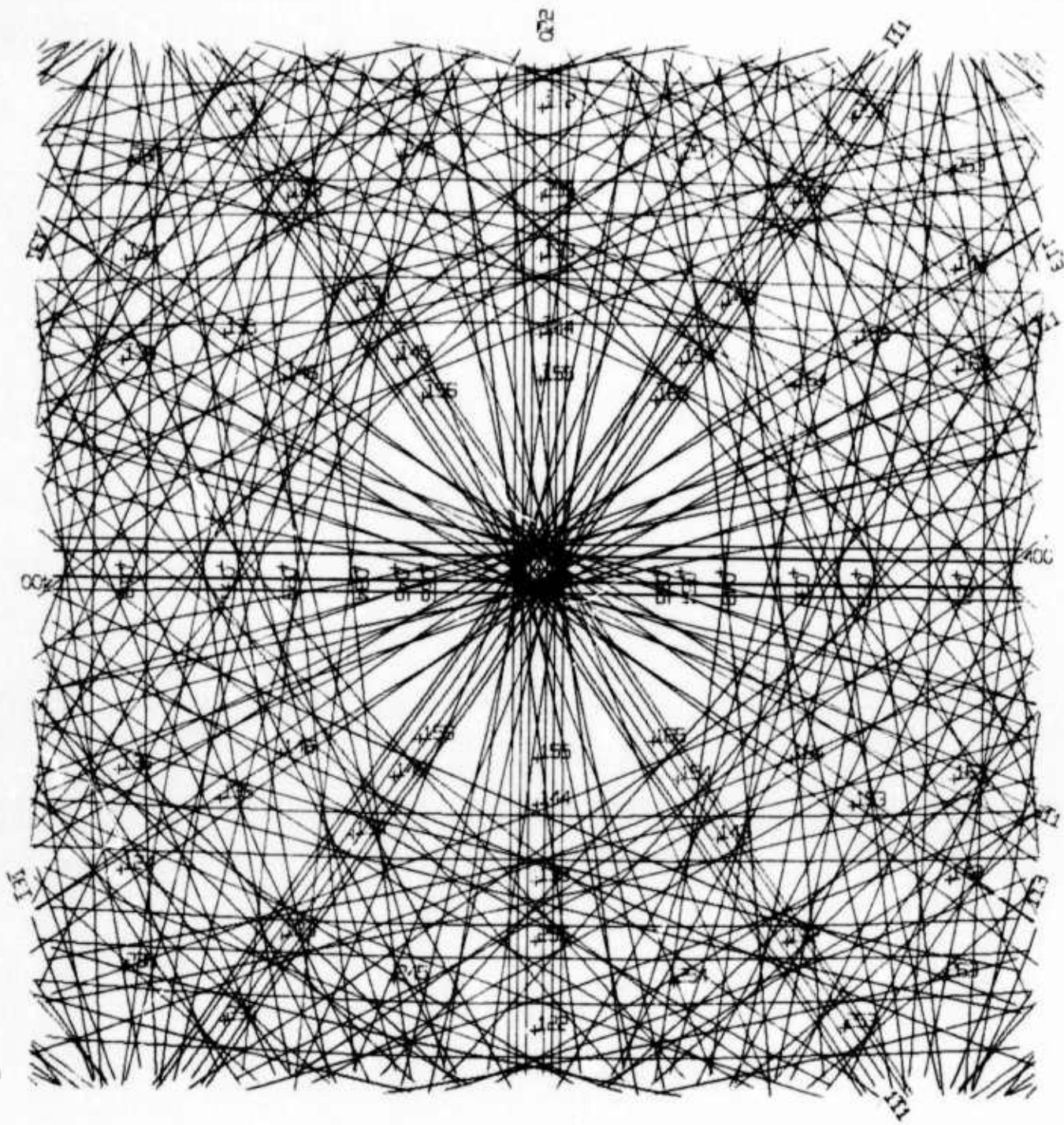


Fig. 10. (011) map for Si 200 keV,  $x_0 = y_0 = 12\text{cm}$ ,  $R = 32\text{cm}$ , RMN = 4, SMSQ = 9.

Reproduced from  
best available copy.

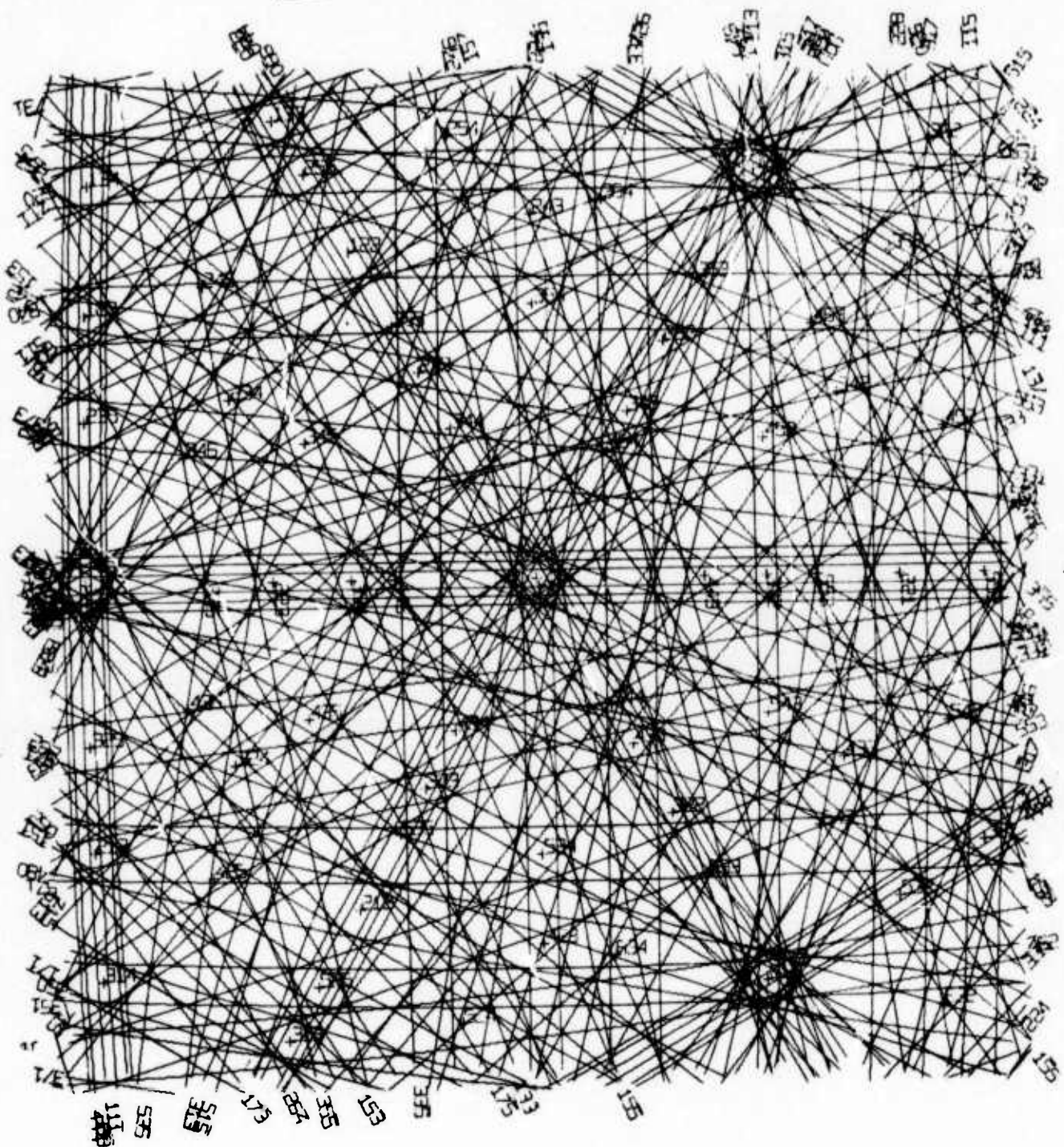


Fig. 11. (111) map for Si 200 keV,  $x_0 = y_0 = 12\text{cm}$ ,  $R = 32\text{cm}$ , RMN = 4, SMSQ = 9.

1. Consider the rotation between micrograph and diffraction pattern that depends on the number of lenses used and their excitation.
2. Orient the Kikuchi plot the same way as the TEM Kikuchi pattern and take negative values of the pole indices as plotted in the map.
3. Rotate a standard stereographic pole map with the same center pole as the Kikuchi plot by  $180^\circ$  in reference to the pole map plotted within the Kikuchi map.

To avoid any other inversion or rotation we have to use both negatives and prints of the micrograph as recorded in the TEM on the screen.

#### THE PROGRAM

The program is written in Fortran IV for an IBM 1800 computer. The time used to generate one plot depends on the number of lines that have to be plotted. For example, the plot shown in Fig. 4 takes less time than the plot shown in Fig. 6, where higher order and higher index lines appear. The time for the plot in Fig. 6 was about 50 min. The attached program was used for this plot. Figures 6-11 show different plots generated with the same program when parameters used are as described in each figure caption.

Steps of the program:

1. Selection of diffraction planes

The usual structure factor equation:

$$F = \sum_{j=1}^n f_j \exp [2\pi i (u_j h + v_j k + w_j l)] \quad (1)$$

is used to calculate the structure factors for silicon so that the planes can be selected which give the Bragg reflections. For this calculation the coordinates  $u$ ,  $v$ ,  $w$  of the position of the 8 atoms in the Si unit cell have to be put into (1). The Bragg equation is used in the form

$$\theta_{hkl} = \frac{\lambda}{2a} \sqrt{h^2 + k^2 + l^2} = 0.0023 \sqrt{h^2 + k^2 + l^2} \quad (2)$$

for 200 keV electrons and Si samples to calculate the Bragg angles  $\theta_{hkl}$  for each plane.

2. Transition to desired orientation with coordinates  
X31, X32, X33

The coordinate transformation

$$\begin{pmatrix} XH \\ XU \\ XL \end{pmatrix} = \begin{pmatrix} h_1/\sqrt{s_1} & k_1/\sqrt{s_1} & l_1/\sqrt{s_1} \\ h_2/\sqrt{s_2} & k_2/\sqrt{s_2} & l_2/\sqrt{s_2} \\ h_3/\sqrt{s_3} & k_3/\sqrt{s_3} & l_3/\sqrt{s_3} \end{pmatrix} \begin{pmatrix} XHS \\ XUS \\ XLS \end{pmatrix} \quad (3)$$

is used where  $(h_3, k_3, l_3) = (X_{31}, X_{32}, X_{33})$ . The other vectors  $(h_1, k_1, l_1)$  and  $(h_2, k_2, l_2)$  have to be chosen in accordance with a right-handed Cartesian system.

$$s_i = h_i^2 + k_i^2 + l_i^2.$$

### 3. Rejection of high-index and high-order planes

Planes of high-index numbers larger than a maximum number  $SMSQ = \sqrt{h^2 + k^2 + l^2}$  have to be rejected; the same is true for planes of higher order than maximum order RMN.

### 4. Calculation of coordinates in the projection plane

The coordinates of one intersection point of the diffraction cone with the projection sphere have to be calculated. For this purpose spherical polar coordinates are introduced. Then the calculation of the coordinates within the projection plane has to be performed by the equation

$$P_x' = 2R \tan \gamma/2 \frac{P_x'}{(P_x'^2 + P_y'^2)^{1/2}} \quad (4)$$

$$P_y' = 2R \tan \gamma/2 \frac{P_y'}{(P_y'^2 + P_z'^2)^{1/2}}$$

where  $\gamma = \cos^{-1} (P_z'/R)$ , as can be seen from Fig. 3.

5. Determination of the radius and center of the Kikuchi circle

From Fig. 3 it can be deduced that the radius of the Kikuchi circle is

$$\overline{CA} = 1/2 (\overline{BO} + \overline{OA}) \quad (5)$$

and the coordinates of the circle center C are

$$CX = P_x (\overline{CO}/\overline{PO})$$

$$CY = P_y (\overline{CO}/\overline{PO})$$

6. Provision for an (x,y) array for the plot

Only a small part of the Kikuchi circle in an area with radius  $RI = \sqrt{(X_0 \times X_0 + Y_0 \times Y_0)}$  around the center pole has to be plotted. Therefore it has to be checked whether a particular Kikuchi circle has a part of it inside this area. Then the circle equation

$$[X - CX]^2 + [Y - CY]^2 = R^2 = [\overline{CA}]^2 \quad (6)$$

is used to provide an array of 50 (x,y) pairs for the plotter.

7. Plotting section

A final check is made to find out which values of the array are inside the plotting square given by  $X_0$  and  $Y_0$ . The

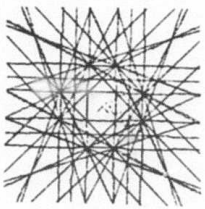
slope of the lines near the border of this square is determined in order to plot the indices of this Kikuchi line pair at the end of the line with the same slope.

#### 8. Plotting the pole map

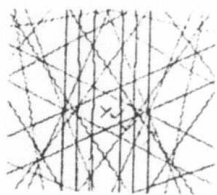
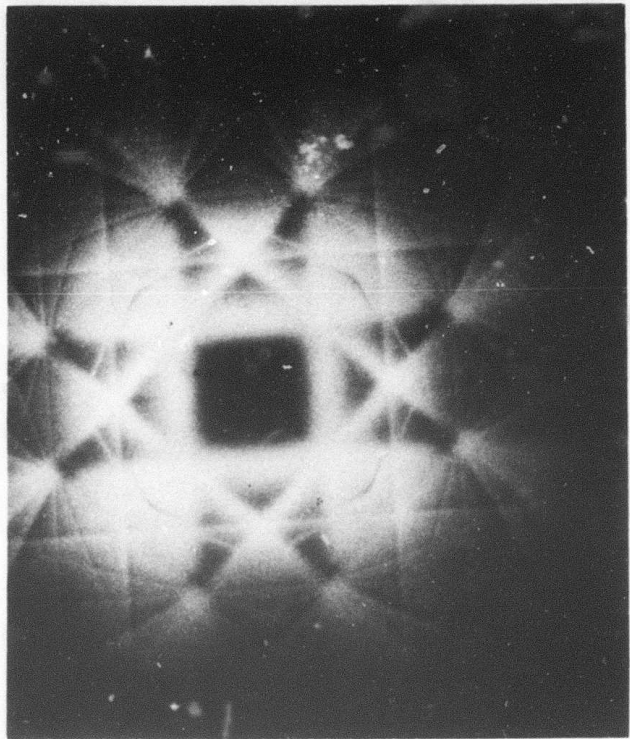
An extra program was written to produce pole maps of the same scale as the Kikuchi map. The steps are essentially similar to steps 2, 3, and 4 above.

### RESULTS

The size of each plot is about  $24 \times 24 \text{ cm}^2$ , which is the maximum usable size of the plotter used. The numbers inside the map represent the indices of the pole where the location is indicated by a +. The numbers outside the map represent the indices of a certain Kikuchi line pair. The indices are plotted at one end of the respective Kikuchi line with the same slope as the lines at this end. Figures 4, 5, 6, and 7 represent (001), (011), and (111) Kikuchi maps with the same scale for Si with 200 keV electrons. Figures 8, 10, and 11 again represent (001), (011), and (111) Kikuchi maps for Si with 200 keV electrons but for about three times larger scale and with higher-order and higher-index lines. Figure 5 is a larger scale plot of the lower-right quadrant of Fig. 4; and Fig. 9 is the same plot as Fig. 8 but with 30 keV electrons and can be used as a map for channeling pattern for the SEM. Figure 12 gives several examples of Kikuchi poles as shown on the maps and in the TEM.



(001) pole



(114) pole

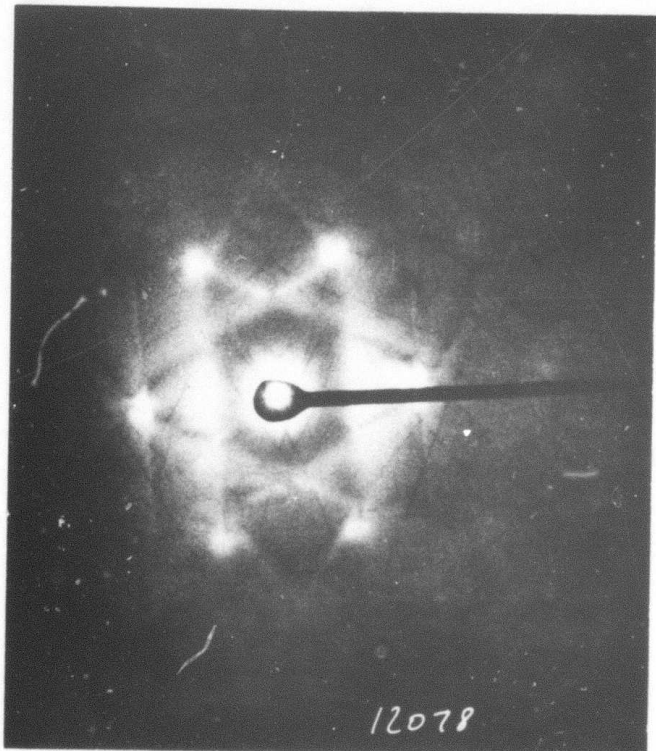
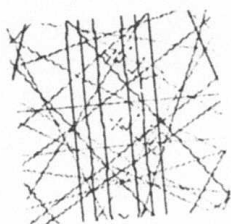
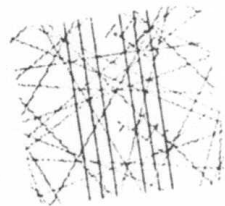
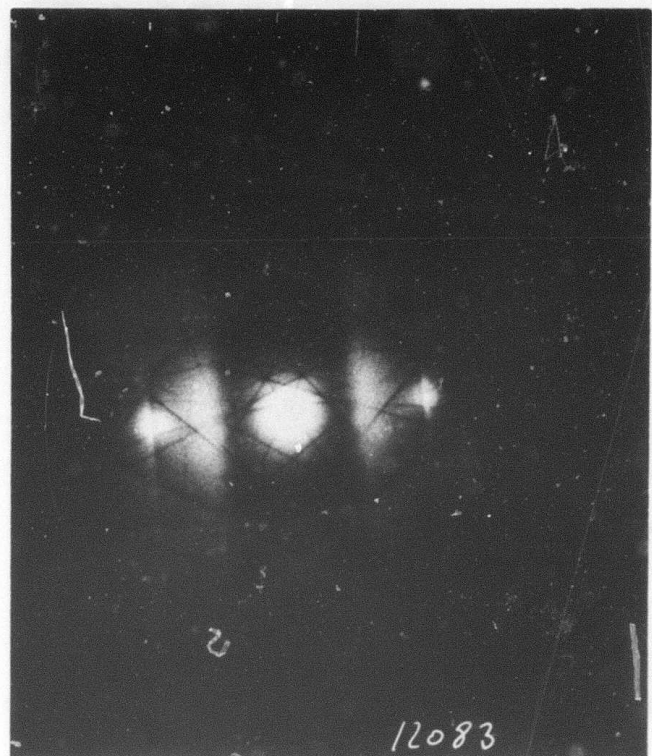


Fig. 12. Kikuchi poles of Si with 200 keV electrons as shown on the map of Fig. 5 and in the Hitachi TEM.



(116) pole



(115) pole

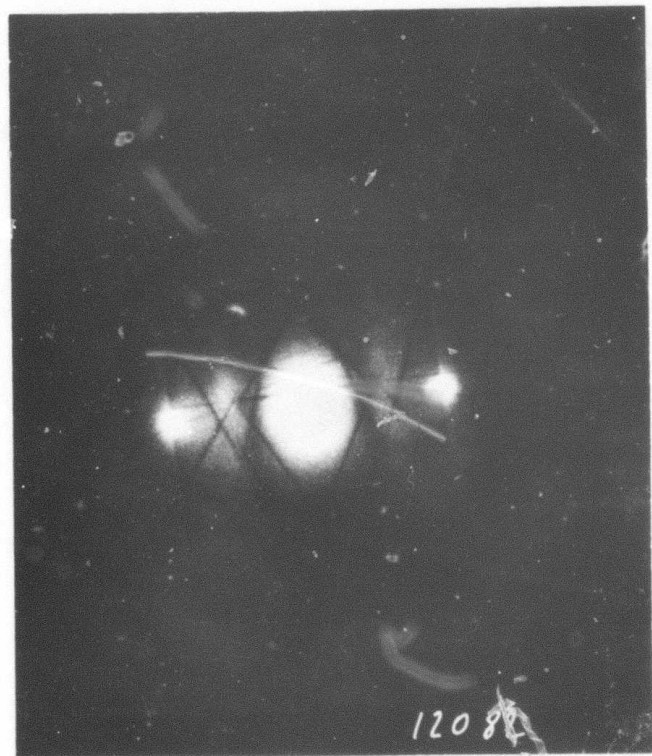


Fig. 12. Kikuchi poles of Si with 200 keV electrons as shown on the map of Fig. 5 and in the Hitachi TEM.

## ACKNOWLEDGMENT

The author wishes to thank R. Anderson and G. Das for helpful discussions

## REFERENCES

1. P. B. Hirsch et al., Electron Microscopy of Thin Crystals, Butterworths, 1965.
2. S. Amelinckx et al., Modern Diffraction and Imaging Techniques in Material Science, North Holland, 1970.
3. L. E. Murr, Electron Optical Applications in Materials Science, McGraw Hill, 1970.
4. E. Levine et al., J. Appl. Phys. 37, 2141 (1966).
5. P. R. Okamoto et al., J. Appl. Phys. 38, 289 (1967).
6. M. V. Heimendahl, Phys. Stat. Sol. (a) 5, 137 (1971).
7. J. C. Bomback and L. E. Thomas, J. Appl. Cryst. 4, 356 (1971).
8. W. K. Wu and J. Washburn, J. Appl. Phys. 45, 1085 (1974).
9. C. T. Young and J. L. Lytton, J. Appl. Phys. 43, 1408 (1972).
10. A. K. Head et al., Computed Electron Micrographs and Defect Identification, North Holland, 1973.

## APPENDIX—FORTRAN IV PROGRAM

```

// JOB      Y    02 JAN 70 20.331 HRS
// FOR PROG 02 JAN 70 20.331 HRS
*10CS(CARD, 1443 PRINTER)
*I0CS (PLOTTER)
*TRANSFER TRACE
*ARITHMETIC TRACE
*LIST ALL
*ONE WORD INTEGERS
INTEGER H,HI,H1A,HA
DIMENSION U(8),V(8),W(8),CX(2),CY(2),RKC(2),
1X(50),Y(50),XP(50),YP(50),SF(17,17,9)

C READ LATTICE PARAMETER
C
DO 10 I=1,8
  READ (2,7) U(I),V(I),W(I)
 7 FORMAT (3F6.2)
10 CONTINUE
C
C READ R OF STEREO SPHERE
C
READ (2,8) R
 8 FORMAT (1F6.2)
C RI=RADIUS OF PLOTTING CIRCLE, XO,YO PLOTTING SQUARE
C
C RI=12.5
C YO=12.5
C Q1=SQR(T(XO**X0+YO**YO))
C
C PRODUCE (H,K,L) VALUES
C
C 00 19 H=1,9
C H1=H-1
C DO 29 K=1,9
C K1=K-1
C DO 39 L=1,9
C L1=L-1
C
C CALCULATE STRUCTURFACTOR
C
C F1=0.0
C F2=0.0
C THET=0.0
C DO 50 M=1,8
C A=6.28*(U(M)*H1+V(M)*K1+W(M)*L1)
C F1=F1+COS(A)
C F2=F2+SIN(A)
C
C 50 CONTINUE
C F=ROUND((F1**2+F2**2)**2)
C SF(H,K,L)=F
C
C 39 CONTINUE
C 29 CONTINUE
C 19 CONTINUE
C XSCAL=0.39
C YSCAL=XSCAL
C CALL SCALF (XSCAL,YSCAL,0.0,0.0,0.0)
C
C 20 H=1,17

```

```
H1=H-9
H1A=IABS(H1)+1
DO 30 K=1,17
K1=K-9
K1A=IABS(K1)+1
DO 40 L=1,17
L1=L-9
L1A=IABS(L1)+1
F=SF(IH1A,K1A,L1A)
IF(F-1.) 4C,40,60
60 S0=SQRT(IFLOAT(H1*H1+K1*K1+L1*L1))
C BRAGG ANGLE 200 KV LAMBDA=0.0251 AE, SI A=5.4308 AE
C THET=0.0023*S0
C
C SELECT PLANES OF LOW INDEX
C
C SMSQ=5.
C IF(SMSQ-SQ) 40,40,140
C CALCULATE COORDINATES ON STEREO SPHERE
C FOR POL. I:I1,K1,L1)
C
C 140 IF (SQ-0.5) 40,40,141
C     XHS=R*H1/SQ
C     XKs=R*K1/SQ
C     XLS=R*L1/SQ
C
C TRANSITION TO DESIRED ORIENTATION WITH COORD. X31,X32,X33
C
C     X11=1.
C     X12=0.
C     X13=0.
C     X21=0.
C     X22=1.
C     X23=-1.
C     X31=0.
C     X32=1.
C     X33=1.
C
C     S1=SQRT(X11*X11+X12*X12+X13*X13)
C     S2=SQRT(X21*X21+X22*X22+X23*X23)
C     S3=SQRT(X31*X31+X32*X32+X33*X33)
C     A11=X11/S1
C     A12=X12/S1
C     A13=X13/S1
C     A21=X21/S2
C     A22=X22/S2
C     A23=X23/S2
C     A31=X31/S3
C     A32=X32/S3
C     A33=X33/S3
C     XH=A11*XHS+A12*XKS+A13*XLS
KIKU0123
KIKU0123
KIKU0124
KIKU0125
KIKU0125
KIKU0126
KIKU0126
KIKU0127
KIKU0127
KIKU0128
KIKU0129
KIKU0190
KIKU0195
KIKU0200
KIKU0205
KIKU0300
KIKU0305
KIKU0310
KIKU0320
KIKU0360
KIKU0362
KIKU0364
KIKU0365
KIKU0366
KIKU0367
KIKU0368
KIKU0369
KIKU0370
KIKU0371
KIKU0372
KIKU0372
KIKU0375
KIKU0376
KIKU0377
KIKU0378
KIKU0379
KIKU0380
KIKU0381
KIKU0382
KIKU0383
KIKU0385
```

```

XK=A21*XHS+A22*XKS+A23*XLS          KIKU0386
XL=A31*XHS+A32*XKS+A33*XLS          KIKU0387

C REJECT PLANES OF HIGHER ORDER

C 130 Y11=10000.*((H1A-1)+100.*((K1A-1)+(L1A-1))
    00 80 IH=1,5
    IH1=IH-1
    DO 90 IK=1,5
    IK1=IK-1
    00 100 IL=1,5
    IL1=IL-1
    IF(IH1+IK1+IL1) 100,101
101 00 110 N=2,8
    X12=N*(10000.*IH1+100.*IK1+IL1)
    RDXI=X11-X12
    ARDX=ABS(RDXI)
    IF(ARDX-0.1) 45,45,46
    46 IF(RDXI) 100,45,110
    45 00 111 M=1,8
    IH5=IH1*M+1
    IK5=IK1*M+1
    IL5=IL1*M+1
    IG=IH1+IK1+IL1
    IF ((IG) 111,111,43
    43 FH=SF(IH5,IK5,IL5)
    IF(FH-1.) 111,111,41
    111 CONTINUE
    41 RN=FLOAT(N)
    RMN=R(NUNO(IRN/RM))
    IF(RMN-4.) 252,252,40
    110 CONTINUE
    100 CONTINUE
    90 CONTINUE
    80 CONTINUE

C COORDINATES FOR DIFFR.CONE ON SPHERE
C
    252 IF (XH) 253,254,255
    255 A1=XK/XH
    PHI=ATAN(A1)
    GO TO 261
    254 IF (XK) 257,256,256
    256 C=0.
    S=1.
    G1 TO 259
    257 C=0.
    S=-1.
    GO TO 259
    253 IF (XK) 258,260,258
    258 A1=XH/XH
    PHI=ATAN(A1)+3.141593
    GO TO 261

```

```

260 C=-1.
      S=0.
      GO TO 259
261 C=COS(PHI)
      S=SIN(PHI)
259 IF (XL) 265,262,263
262 TH=1.570796
      GO TO 264
263 A2=SORT((R/XL)**2-1.)
      TH=ATAN(A2)
      GO TO 264
265 A2=-SORT((R/XL)**2-1.)
      TH=ATAN(A2)
      IF (TH) 266,266,264
266 TH=TH+3.141593
      C
264 ARG12=TH+1.570796-THET
      S12=SIN(ARG12)
      C12=COS(ARG12)
      XH12=R*C*S12
      XK12=R*S*S12
      XL12=R*C12
      KIKU0462
      KIKU0463
      KIKU0464
      KIKU0465
      KIKU0466
      KIKU0466
      KIKU0467
      KIKU0468
      KIKU0469
      KIKU0470
      KIKU0471
      KIKU0472
      KIKU0473
      KIKU0473
      KIKU0473
      KIKU0474
      KIKU0475
      KIKU0482
      KIKU0485
      KIKU0490
      KIKU0495
      KIKU0500
      KIKU0505
      KIKU0510
      KIKU0515
      KIKU0520
      KIKU0525
      KIKU0530
      KIKU0535
      KIKU0540
      KIKU0545
      KIKU0550
      KIKU0555
      KIKU0560
      KIKU0565
      KIKU0566
      KIKU0567
      KIKU0568
      KIKU0569
      KIKU0570
      KIKU0575
      KIKU0580
      KIKU0585
      C
      CALCULATE COORDINATES IN PROJECTION PLANE
      C FOR DIFFR. CONE
      C
      A12=SORT((R/XL12)**2-1.)
      IF (XL12) 271,2710,272
271 GAM12=(3*141593-ATAN(A12))/2.
      GO TO 273
272 GAM12=ATAN(A12)/2.
      GO TO 273
2710 GAM12=0.785398
      273 TAN12=SIN(GAM12)/COS(GAM12)
      KIKU0605
      KIKU0606
      KIKU0607
      KIKU0608
      KIKU0609
      KIKU0611
      KIKU0613
      KIKU0615
  
```

F12=2.\*R\*TAN12/SQRT(XH12\*XH12+XK12\*XK12)

A1X=XH12\*F12  
A1Y=XK12\*F12

C A21=SQRT((R/XL21)\*\*2-1.)  
IF(XL21) 274,2740,275  
274 GAM21=(3.141593-ATAN(A21))/2.  
GO TO 276  
275 GAM21= ATAN(A21)/2.  
GO TO 276

2740 GAM21=0.785398  
276 TAN21=SIN(GAM21)/COS(GAM21)  
F21=2.\*R\*TAN21/SQRT(XH21\*XH21+XK21\*XK21)  
81X=XH21\*F21  
81Y=XK21\*F21

C A11=SQRT((R/XL11)\*\*2-1.)  
IF(XL11) 278,2780,279  
278 GAM11=(3.141593-ATAN(A11))/2.  
GO TO 280  
279 GAM11= ATAN(A11)/2.  
GO TO 280

2780 GAM11=0.785398  
280 TAN11=SIN(GAM11)/COS(GAM11)  
F11=2.\*R\*TAN11/SQRT(XH11\*XH11+XK11\*XK11)  
A2X=XH11\*F11  
A2Y=XK11\*F11

C A22=SQRT((R/XL22)\*\*2-1.)  
IF(XL22) 281,2810,282  
281 GAM22=(3.141593-ATAN(A22))/2.  
GO TO 283  
282 GAM22= ATAN(A22)/2.  
GO TO 283

2810 GAM22=0.785398  
283 TAN22=SIN(GAM22)/COS(GAM22)  
F22=2.\*R\*TAN22/SQRT(XH22\*XH22+XK22\*XK22)  
82X=XH22\*F22  
82Y=XK22\*F22

C CALCULATE RADIUS AND COORDINATES OF KKC RKC1 AND RKC2

C A8X1=B1X-A1X  
A8Y1=B1Y-A1Y  
ABX2=B2X-A2X  
ABY2=B2Y-A2Y

C RKC(1)=0.5\*SQRT(ABX1\*A8X1+ABY1\*A8Y1)  
CX(1)=(A1X+81X)/2.  
CY(1)=(A1Y+81Y)/2.

C RKC(2)=0.5\*SQRT(A8X2\*ABX2+A8Y2\*ABY2)  
CX(2)=(A2X+82X)/2.  
CY(2)=(A2Y+82Y)/2.  
WRITE(5,6968) HI,K1,L1,RKC(1),CX(1),CY(1),RKC(2),CX(2),CY(2)

KIKU0620  
KIKU0625  
KIKU0630  
KIKU0635  
KIKU0636  
KIKU0637  
KIKU0638  
KIKU0639  
KIKU0641  
KIKU0643  
KIKU0645  
KIKU0648  
KIKU0650  
KIKU0655  
KIKU0660  
KIKU0661  
KIKU0662  
KIKU0663  
KIKU0664  
KIKU0666  
KIKU0668  
KIKU0670  
KIKU0675  
KIKU0680  
KIKU0685  
KIKU0690  
KIKU0691  
KIKU0692  
KIKU0693  
KIKU0694  
KIKU0695  
KIKU0698  
KIKU0700  
KIKU0705  
KIKU0710  
KIKU0715

6968 FORMAT (2X,3I3,2X,6F12.2)

C CHECK INTERSECTION OF PLOT CIRCLE WITH KC

```

C DO 500 I=1,2
      SCH=.5*(R1*R1+CX(I)*CX(I)+CY(I)*CY(I))-RK(I)*RK(I)
      R11=CY(I)*CX(I)+CY(I)*CY(I)
      SCH1=(CY(I)*CX(I)*R11*R1-SCH)*SCH/R11+(SCH*CX(I)/R11)**2
      IF (SCH1) 401,410,410
  401  SCH2=SCH1+.5*E-5
      IF (SCH2) 40,410,402
  402  SCH1=0.0

C CALCULATE INTERSECTION
C
 410  SQS=SQRT(SCH1)
      X1=SCH*CX(I)/R11 +SQS
      X2=SCH*CX(I)/R11-SQS
      Y1=SQRT(R1*R1-X1*X1)
      Y2=SQRT(R1*R1-X2*X2)
      T1=RK(I)-SQRT((X1-CX(I))**2+(Y1-CY(I))**2)
      T1A=ABS(T1)
      IF (T1A-0.01) 430,430,420
  420  Y1=-Y1
  430  T2=RK(I)-SQRT((X2-CX(I))**2+(Y2-CY(I))**2)
      T2A=ABS(T2)
      IF (T2A-0.01) 441,441,440
  440  Y2=-Y2
      GO TO 450
  441  RY=ABS(Y1-Y2)-0.1
      IF (RY) 449,449,450
  449  Y2=-Y2
  450  XIS=X1-CX(I)
      X2S=X2-CX(I)
      Y1S=Y1-CY(I)
      Y2S=Y2-CY(I)
      IF (X1S) 505,510,515
  515  IF (Y1S) 517,516,516
  516  ALF1=ATAN(Y1S/X1S)
      GO TO 528
  517  ALF1=ATAN(Y1S/X1S)+6.283186
      GO TO 528
  510  IF(Y1S) 520,523,526
  526  ALF1=1.570796
      GO TO 528
  523  ALF1=0.
      GO TO 528
  520  ALF1=4.712389
      GO TO 528
  505  ALF1=ATAN(Y1S/X1S)+3.141593
  528  IF(X2S) 525,530,535
  535  IF(Y2S) 537,536,536
  536  ALF2=ATAN(Y2S/X2S)
      GO TO 5450
  537  ALF2=ATAN(Y2S/X2S)+6.283186

```

```

GO TO 5450
530 IF(Y2S) 540,543,546
546 ALF2=1.57
      GO TO 5450
543 ALF2=0.
      GO TO 5450
540 ALF2=4.712389
      GO TO 5450
525 ALF2=ATAN(Y2S/X2S)+3.141593
5450 IF(X1S) 5451,5451,5452
5452 IF(X2S) 5451,5451,5453
5453 IF(Y1S) 5455,5451,5454
5454 IF(Y2S) 5456,5451,5451
5456 ALF2=ALF2-6.283186
      GO TO 5451
5455 IF(Y2S) 5451,5451,5458
5458 ALF1=ALF1-6.283186
5451 DALF=(ALF1-ALF2)/50.
      J=0
      D0 600 M1=1,50
      IF(H1)5501,5501,5502
5501 M=M1
      GO TO 5503
5502 M=51-M1
5503 X(M)=RK(C(I)*COS(ALF1-DALF*(M-1))+CX(I)
      Y(M)=RK(C(I)*SIN(ALF1-DALF*(M-1))+CY(I)
      AX=ABS(X(M))
      AY=ABS(Y(M))
      IF(X0-AX) 600,550,550
      550 IF(Y0-AY) 600,580,580
      580 J=J+1
      XP(J)=X(M)
      YP(J)=Y(M)
      600 CONTINUE

C PLOTTING SECTION
C
      IF(J=2) 500,699,699
      699 CALL FPLOT (-2,XP(1),YP(1))
      WRITE(5,69962) H,K,L
6992 FORMAT (8X,3I3)
      DC 700 JJ=1,J
700 CALL FPLOT (0,XP(JJ),YP(JJ))
      CALL FPLOT (-1,XP(J),YP(J))
      IF(J=1) 500,500,7000
      7000 DY=YP(J)-YP(J-2)
      DX=XP(J)-XP(J-2)
      IF(DX) 7012,7011,7010
      7010 DEL=ATAN(DY/DX)
      GO TO 7020
      7011 DEL=0.0
      GO TO 7020
7012 DEL=ATAN(DY/DX)+3.141593
      7020 XB=XP(J)+0.5*COS(DEL)
      YB=YP(J)

```

```

HA=IABS(H1)
KA=IABS(K1)
LA=IABS(L1)
CALL FCHAR(XB,YB,.1,.12,DEL)
WRITE(11,7099) HA,KA,LA
7099 FORMAT (3I1)
XB=XB-0.35*SIN(DEL)
YB=YB+0.35*COS(DEL)
DXB=0.25*COS(DEL)
DYB=0.25*SIN(DEL)
XB=XB1+DXB
YB=XB1+DYB
XB=XB1+2.*DXB
YB=YB1+2.*DYB
XB=XB1+3.*DXB
YB=XB1+3.*DYB
IF(H1)7061,7060,7060
7061 CALL FPLOT(-2,XB1,YB1)
CALL FPLOT(-1,XB2,YB2)
7060 IF(K1)7071,7070,7070
7071 CALL FPLOT(-2,XB2,YB2)
CALL FPLOT(-1,XB3,YB3)
7070 IF(L1)7081,40,40
7081 CALL FPLOT(-2,XB3,YB3)
CALL FPLOT(-1,XB4,YB4)
500 CONTINUE
40 CONTINUE
30 CONTINUE
20 CONTINUE
CALL EXIT
END

```

## VARIABLE ALLOCATIONS

V(R )=000E-0000	W(R )=001E-0010	CX(R )=0032-0030	CY(R )=0036-0034
X(R )=009E-003C	Y(R )=0102-00A0	YP(R )=01CA-0168	SF(R )=003A-003
XO(R )=1620	YO(R )=1622	F1(R )=1626	R(R )=161E
A(R )=162C	F(R )=162E	YSCL(R )=1632	THET(R )=162A
XHS(R )=1638	XKS(R )=163A	X11(R )=163E	SMOD(R )=1635
X21(R )=1644	X22(R )=1646	X31(R )=164A	X13(P )=1642
S1(R )=1650	S2(R )=1652	X32(R )=164C	X35(R )=164E
A21(R )=165C	A22(R )=165E	A11(R )=1656	A13(R )=165A
XH(R )=1668	XK(R )=166A	A31(R )=1662	A33(iR )=1665
ARDX(R )=1674	FH(R )=1676	X11(R )=166E	RDX1(R )=1672
PH1(R )=1680	C(R )=1682	RM(R )=167A	A1(R )=167E
S12(R )=168C	C12(R )=168E	RWN(R )=167C	ARG12(R )=168A
S21(R )=1698	C21(R )=169A	TH(R )=1686	ARG21(R )=1696
S11(R )=16A4	C11(R )=16A6	XK12(R )=1692	ARG21(R )=1694
S22(R )=16B0	C22(R )=16B2	XK21(R )=169E	XL12(R )=16A0
TAN12(R )=16BC	F12(R )=16BE	XH11(R )=16AA	XL21(R )=16A2
F21(R )=16C8	B1X(R )=16CA	XH22(R )=16B4	ARG22(R )=16AE
A2X(R )=16D4	A2Y(R )=16D6	A1Y(R )=16C2	GAM12(R )=16B8
B2Y(R )=16E0	ABX1(R )=16E2	GAM21(R )=16C4	TAN11(R )=1600
R11(R )=16EC	SCH1(R )=16EE	TAN11(R )=16CE	F11(R )=1602
Y1(R )=16F6	Y2(R )=16FA	TAN22(R )=16DA	B2X(R )=16DC
RY(R )=1704	X1S(R )=1706	ABY1(R )=16E4	ABY2(R )=16EB
		*BX2(R )=16E6	SCH(R )=16EA
		SCH2(R )=16F0	X2(R )=16F4
		T1(R )=16FC	T2(R )=1700
		Y1S(R )=1708	Y2S(R )=170C

ALF2(R )=1710	DALF(R )=1712	AX(R )=1714	AY(R )=1716	DY(R )=1718
DEL(R )=171C	X8(R )=171E	Y8(R )=1720	X81(R )=1722	YB1(R )=1724
DYB(R )=1728	X82(R )=172A	Y82(R )=172C	X83(R )=172E	YB3(R )=1730
Y84(R )=1734	H(I )=1740	H1(I )=1741	HA(I )=1742	I(I )=1744
K(I )=1745	K1(I )=1746	L(I )=1747	L1(I )=1748	K1A(I )=1749
L1A(I )=1748	IH(I )=174C	IH1(I )=174D	IK(I )=174E	K1I(I )=174F
IL1(I )=1751	N(I )=1752	IH5(I )=1753	IK5(I )=1754	IL(I )=1750
J(I )=1757	M1(I )=1758	JJ(I )=1759	KA(I )=175A	IG(I )=1756

STATEMENT ALLOCATIONS

7 =179E 8	=17A1	6968 =17A3	6962 =17AA	7099 =17AE	10 =17C4	50 =184A	39 =1873	29 =187C	19 =1885
60 =18E5	140 =1917	141 =191E	130 =1A2C	101 =1A70	46 =1AA4	45 =1AA8	43 =1AD7	111 =1AE8	41 =1AF
110 =1D12	100 =1818	90 =1824	80 =182D	252 =1836	255 =183D	254 =184A	256 =1B4F	257 =1B59	253 =1B64
258 =1869	260 =1878	261 =1883	259 =188D	262 =1894	263 =189A	265 =18B0	266 =18BCA	264 =18CA	271 =1C26
272 =1C91	2710 =1C9A	273 =1C9E	274 =1CE9	275 =1CF4	2740 =1CFD	276 =1D01	278 =1D57	279 =1D67	2780 =1D68
280 =10E4	281 =1DAF	282 =1DRA	283 =1OC3	284 =1DC7	401 =1E4	402 =1EF1	410 =1EF5	420 =1F6C	430 =1F7L
440 =1FA7	441 =1FAE	449 =1FC0	450 =1FC5	515 =1FEF	516 =1FF4	517 =2001	510 =2010	526 =2017	523 =201N
520 =2023	505 =2029	528 =2036	535 =2030	536 =2042	537 =204F	530 =2054	546 =2065	543 =2058	540 =207
525 =2077	5450 =2084	5453 =2089	5454 =208E	5455 =2095	5456 =209A	5455 =20A2	5458 =20A7	5451 =20AD	5501 =20C2
5502 =20C8	5503 =20CE	550 =212D	580 =2134	600 =2152	699 =2162	700 =2188	7000 =21D7	7010 =21FC	7011 =2209
7012 =220F	7020 =221C	7061 =22A3	7060 =22B7	7071 =228C	7070 =22D0	7081 =22D5	500 =22E9	40 =22F2	30 =22F8
20 =2304									

FEATURES SUPPORTED  
 TRANSFER TRACE  
 ARITHMETIC TRACE  
 ONE WORD INTEGERS  
 IDCs

CALLED SUBPROGRAMS	F SORT	F COS	F SIN	ROUND	SCALF	IABS	F ABS	F ATAN	F PLOT	F CHAR	FAOD	F ADDX	F SUBX	F MPY
	F PCOS	F DIV	F LD	F LDX	F STO	F SBR	F SBRX	F DVR	F AXI	F M ARX	F M ARX	F FLOAT	F HI F	F MIF
	F MPYX			M IOFX	M IOF	M IOI	SUBSC	SNR	F CHRI	HOLEB	PRNTN	E PRPT	CARDN	
REAL CONSTANTS														
	*.25000E 02=1760		.000000E 00=1762		*.628000E 01=1764		*.390000E 00=1766		*.100000E 01=1768		*.230000E -02=176A			
	*.50000E 01=176C		*.500000E 00=176E		*.100000E 05=1770		*.100000E 03=1772		*.100000E 00=1774		*.400000E 01=1776			
	*.314159E 01=1778		*.157079E 01=177A		*.200000E 01=177C		*.785398E 00=177E		*.500000E -04=1780		*.100000E -01=1782			
	*.628318E 01=1784		*.471239E 01=1786		*.157000E 01=1788		*.500000E 02=178A		*.120000E 00=178C		*.350000E 00=1785			
INTEGER CONSTANTS														
	1=1794	8=1795	2=1796	9=1797	17=1798	5=1799	0=179A	50=1798	51=179C	11=1797				

CORE REQUIREMENTS FOR PROG  
 COMMON 0 INSKEL COMMON 0  
 VARIARLES 5984 PROGRAM 2992

```

// FOR PROG 02 JAN 70 20.079 HRS
*10CS(CARD, 1443 PRINTER)
*JDCS (PLOTTER)
*TRANSFER TRACE
*ARITHMETIC TRACE
*LIST ALL
*ONE WORD INTEGERS
INTEGER HZ,HZ1,HZ11,HZA
C RADIUS R OF PROJ. SPHERE
C
C R=11.
XSCAL=0.39
YSCAL=XSCAL
CALL SCALF(XSCAL,YSCAL,0.0,0.0)
C SIZE OF MAP 2*X0*2*Y0 CM*CM
C
C X0=11.
Y0=11.
DO 300 HZ=7.17
H21=HZ-9
DO 310 KZ=7.17
KZ1=KZ-9
DO 320 LZ=7.17
LZ1=LZ-9
SQ=SORT(IFLOAT(HZ1*HZ1+KZ1*KZ1+LZ1*LZ1))
C REJECT HIGH INDEX POLES
C
SMSQ=4.
IF(SMSQ=50) 320,320,329
329 IF(SQ=0.5) 320,320,351
351 FZ=R/SQ
XHZS=HZ1*FZ
XKZS=KZ1*FZ
X1ZS=LZ1*FZ
C TRANSITION TO DESIRED ORIENTATION WITH COORD. X31,X32,X33
C
X11=1.
X12=0.
X13=0.
X21=0.
X22=1.
X23=-1.
X31=0.
X32=1.
X33=1.
S1=SORT(X11*X11+X12*X12+X13*X13)
S2=SORT(X21*X21+X22*X22+X23*X23)
S3=SORT(X31*X31+X32*X32+X33*X33)
A11=X11/S1
A12=X12/S1
A13=X13/S1
A21=X21/S2
A22=X22/S2
A23=X23/S2

```



```

A31=X31/S3 KIKU6074
A32=X32/S3 KIKU6075
A33=X33/S3 KIKU6076
XHZ=A1*XHZS+A12*XKZS+A13*XLSZS KIKU6080
XHZ=A21*XHZS+A22*XKZS+A23*XLSZS KIKU6081
XLZ=A31*XHZS+A32*XKZS+A33*XLSZS KIKU6082
IF (XLZ) 320,301,301 KIKU6085

C REJECT HIGH ORDER POLES

C 301 HZA=ABS(HZ1) KIKU6090
KZA=ABS(KZ1) KIKU6052
LZA=ABS(LZ1) KIKU6053
X11=1000.*HZ A+100.*KZA+LZA KIKU6054
D0 340 IH=1,5 KIKU6055
IH1=IH-1 KIKU6056
D0 341 IK=1,5 KIKU6057
IK1=IK-1 KIKU6058
D0 342 IL=1,5 KIKU6059
IL1=IL-1 KIKU6060
D0 343 N=2,8 KIKU6061
IF (IH1+IK1+IL1) 344,342,344 KIKU6062
344 X12=N*(10000.*IH1+100.*IK1+IL1) KIKU6063
RX1=X11-X12 KIKU6064
IF (RX1) 342,320,343 KIKU6065
343 CONTINUE KIKU6066
342 CONTINUE KIKU6067
341 CONTINUE KIKU6068
340 CONTINUE

C CALCULATE COORD. IN PROJECTION PLANE

C
A2=SQRT((R/XLZ)**2-1.) KIKU6110
IF (XLZ) 354,353,352 KIKU6112
354 GAMZ=(3.141592653589793-ATAN(A2))/2. KIKU6114
GO TO 356 KIKU6116
352 GAMZ=ATAN(AZ)/2. KIKU6118
GO TO 356 KIKU6120
353 GAMZ=0.785398 KIKU6122
356 TANZ=SIN(GAMZ)/COS(GAMZ) KIKU6130
SORA=SORT(XHZ*XHZ+XKZ*XKZ) KIKU6135
IF (SORA-0.5) 359,359,355 KIKU6138
355 FZ1=2.*R*TANZ/SORA KIKU6140
PXZ=XHZ*FZ1 KIKU6150
PYZ=XKZ*FZ1 KIKU6160
GO TO 358 KIKU6162
359 AXLZ=ARS(XLZ) KIKU6164
IF (AXLZ-0.5) 320,320,357 KIKU6166
357 PXZ=0.0 KIKU6168
PYZ=0.0 KIKU6169
358 APXZ=ABS(PXZ) KIKU6170
APYZ=ABS(PYZ) KIKU6171
C SELECT POINTS WITHIN THE PLOTTED AREA
C

```

```

IF(X0-APXZ) 320,321,321
321 IF(Y0-APYZ) 320,324,324
C PLOT + AND NUMBER (HZ1,KZ1,LZ1) AT COORDINATES (PXZ,PYZ)
C
324 CALL FPLOT (-2,PXZ,PYZ)
CALL POINT (0)
CALL FPLOT (-1,PXZ,PYZ)
HZ1=IABS(HZ1)
KZ1=IABS(KZ1)
LZ1=IABS(LZ1)
IF(APXZ-0.1) 326,326,325
325 CALL FCHAR (PXZ-0.06*XSCAL*PYZ+0.1*YSCAL,.1,.12,.1,571)
WRITE (11,390) HZ11,KZ11,LZ11
390 FORMAT (311)
IF(HZ1) 361,360,360
361 CALL FPLOT (-2,PXZ-0.40,PYZ+0.04)
CALL FPLOT (-1,PXZ-0.40,PYZ+0.24)
360 IF (KZ1) 371,370,370
371 CALL FPLOT (-2,PXZ-0.40,PYZ+0.25)
CALL FFINT (-1,PXZ-0.40,PYZ+0.50)
370 IF (171,374) 376,376,376
381 CALL FFINT (-2,PXZ-0.40,PYZ+0.55)
CALL FPLOT (-1,PXZ-0.40,PYZ+0.80)
GO TO 320
326 CALL FCHAR (PYZ+0.06*XSCAL*PYZ+0.1*YSCAL,.1,.12,0,0)
WRITE (11,391) HZ11,KZ11,LZ11
391 FORMAT(311)
IF(HZ1) 366,365,365
366 CALL FPLOT (-2,PXZ+0.03,PYZ+0.4)
CALL FPLOT (-1,PXZ+0.24,PYZ+0.4)
365 IF (KZ1) 376,375,375
376 CALL FPLOT (-2,PXZ+0.25,PYZ+0.4)
CALL FPLOT (-1,PXZ+0.50,PYZ+0.4)
375 IF(LZ1) 386,320,320
386 CALL FPLOT (-2,PYZ+0.55,PYZ+0.4)
CALL FFINT (-1,PYZ+0.80,PYZ+0.4)
320 CONTINUE
310 CONTINUE
300 CONTINUE
CALL EXIT
END

```

## VARIABLE ALLOCATIONS

R(R )=00000	XSCAL(R )=0002	YSCAL(R )=0004	X0(R )=0096	SQ(R )=000A
SMSQR )=000C	FZ(R )=000E	XH2S(R )=0010	XK2S(R )=0012	X11(R )=0016
X12(R )=0018	X13(R )=001A	X21(R )=001C	X22(R )=001E	X31(R )=0020
X32(R )=6024	X33(R )=0026	S1(R )=0028	S2(R )=002A	A11(R )=002E
A12(R )=0030	A13(R )=0032	A21(R )=0034	A22(R )=0036	A31(R )=003A
A32(R )=0048	A33(R )=0040	XHZ(R )=0040	XLZ(R )=0042	X11(R )=0046
X12(R )=0054	RX1(R )=004A	AZ(R )=004C	GAMZ(R )=004E	SQRA(R )=005
FZ1(R )=0054	PX2(R )=0056	PYZ(R )=0158	AXLZ(R )=005A	APYZ(R )=005E
HZ1(R )=006A	HZ1(R )=0068	HZ1(R )=006C	KZ1(R )=006E	K71(R )=006F
LZ1(R )=0070	LZ1(R )=0071	KZA(R )=0072	LZA(R )=0073	IH(I )=0074
IK1(R )=0076	IK1(R )=0077	IL1(I )=0078	IL1(I )=0079	N(I )=007A

02 JAN 70  
PAGE 004

L211(I)=007C

STATEMENT ALLOCATIONS  
390 =0083 391 =0086 329 r011F 351 =0126 301 =0234 344 =0285 343 =0280 342 =0289 341 =02C2 340 =02C0  
354 =02EA 352 =02F5 353 =02FE 356 =0302 355 =0328 359 =0340 357 =034C 358 =0354 321 =0365 324 =036C  
325 =0399 361 =03BF 360 =03E9 371 =03F0 370 =041C 381 =0421 326 =044F 366 =0475 365 =04A1 376 =04AC  
375 =04D2 386 =04D7 320 =0503 310 =050C 300 =0515

FEATURES SUPPORTED  
TRANSFER TRACE  
ARITHMETIC TRACE  
ONE WORD INTEGERS  
INCS

CALLED SUBPROGRAMS  
SCALF FSORT TABS  
FSSTD FSHR FUVR  
PRNTN EBRT CARDN

REAL CONSTANTS  
•110000E 02=007E •390C00E 00=0080 •000000E 00=0082 •400000E 01=0084 •500000E 00=0086  
•100000E 05=008A •100000E 03=008C •314193E 01=008E •200000E 01=0090 •785398E 00=0092  
•600000E-01=0096 •120000E 00=0098 •157100E 01=009A •400000E 00=009C •400000E-01=009E  
•250000E 00=00A2 •500000E 00=00A4 •800000E 00=00A6 •300000E-01=00A8

INTEGER CONSTANTS  
7=00AA 1=00AB 9=00AC 1=00AO 5=00AE 2=00AF 6=00B0 0=00B1 11=00B2

CORE REQUIREMENTS FOR PROG  
COMMON 0 INSKEL COMMON 0  
VARIABLES 126 PROGRAM 1186 0

END OF COMPIRATION

## **Chapter 2**

### **ELECTRICAL CHARACTERIZATION OF QUASI MOS STRUCTURES ON SILICON**

**by**

**W. R. Fahrner, E. F. Gorey, and C. P. Schneider**

#### **INTRODUCTION**

Junctions are present in important devices, e.g., in buried-channel charge-coupled devices (CCDs) or in silicon on sapphire (SOS)-based integrated circuits. In order to optimize the performance of such a device--speed, transfer efficiency, etc.--the characterization of the electrical properties of the material is desirable. For homogeneous silicon, there are some standard techniques based on metal oxide semiconductor (MOS) capacitance measurements for this purpose. The presence of underlying junctions requires important precautions to be made with the use of MOS-CV measurement techniques.

Owing to the junction, the number of components of the equivalent network increases and the analysis is impeded. It will be shown in this paper how this problem can be solved. When one side of a junction described above is oxidized, a quasi MOS structure results. The equivalent network of such a structure is discussed in this paper, and the conditions for MOS C-V and G-V measurements are given. In the case where the MOS admittance can be measured, the following information can be obtained:

1. The surface-state density  $N_{ss}$  (1), the corresponding capture cross sections (2), the charge density in the oxide (3), and deep energy levels (4).
2. The doping concentration  $N_D$ .
3. The lifetime of the minority carriers (5).

Measurements on epitaxial junctions according to (3) have already been carried out (6) without an adequate theoretical basis.

In this investigation, we are primarily interested in the measurement of lifetime, since this parameter is more sensitive to defects and impurities in the crystal than any other electrical parameter (7). Thus, in the section "Range of Quasi MOS Capacitance Technique," the values for layer and substrate resistivity, dot diameter, oxide thickness, etc., refer to ranges in which such lifetime measurements can be carried out.

#### ANALYSIS OF EQUIVALENT NETWORK

In Fig. 1, a cross section of an oxidized n epitaxial layer on a p<sup>-</sup> substrate is shown. The network of the structure consists of the oxide capacitance  $C_{ox}$ , the distributed layer resistance R of the n-layer, the distributed junction admittance  $Y_J = G_J + j\omega C_J$ , and the distributed substrate resistance  $R_s$ . A net consisting of buried layers each of 2.5 times 2.5 mm<sup>2</sup> area with a spacing of 8 mm is diffused into the substrate prior to epitaxy. The doping profiles underneath A (off the

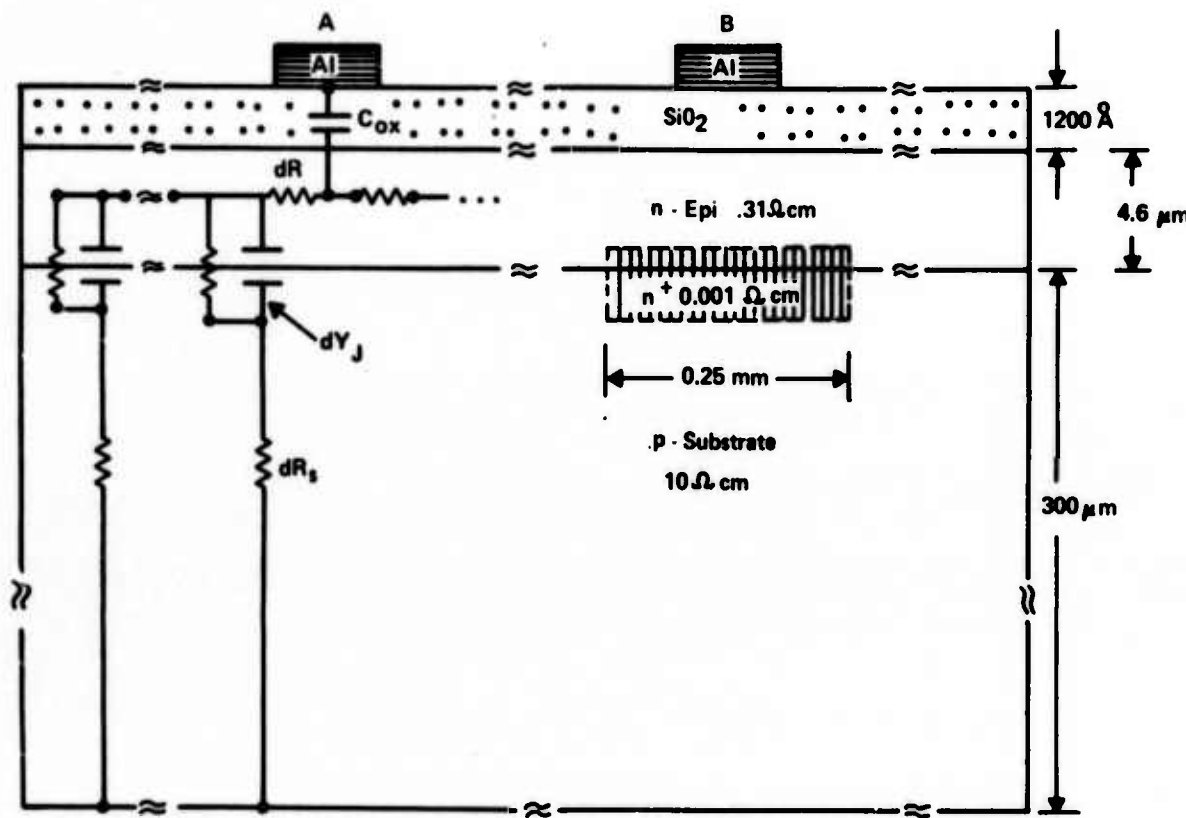


Fig. 1. Cross section of an  $n-p^-$  junction. The  $n$  layer was grown by regular gas phase epitaxy. It is covered by  $1200 \text{ \AA}$  thermal oxide.

buried layer) and B (on the buried layer) are obtained by the spreading resistance technique (Fig. 2). The C-V curves for two dots off the buried layer are shown in Fig. 3. The dots have areas of 0.01765 and 0.00196 cm<sup>2</sup>. The same measurements are repeated for a <115> and a <100> oriented wafer with epitaxial layer resistivity of approximately 0.9 ohm-cm and of approximately 4- $\mu$ m epitaxial thickness. The substrate resistivity is 8 and 6 ohm-cm respectively (Fig. 4a,b). In these wafers, no buried layer is present.

The analysis of the data given in Fig. 3 reveals that the measured low-frequency capacitance in accumulation is identical with the oxide capacitance. This is confirmed through measurements on control wafers, by measuring the oxide thickness and the capacitances for different dot areas and comparing the ratios with the area ratios.

The dc voltage drop ( $v_J$ ) across the junction is 0 since there is no dc current flow through the MOS structure.

The ac admittance is given by  $G_J(v_J) + j\omega C_J(v_J)$  with  $v_J = 0$ .  $G_J$  can be derived as  $G_J = dI_J/dv_J = I_o \times (q/kT) \times \exp(qv_J/kT)$ . In anticipation of the results, the lifetime of the epitaxial layer (which is heavily doped compared with the substrate and can be expected to give the major contribution to the dark current) is measured now to be approximately 1  $\mu$ sec. With this

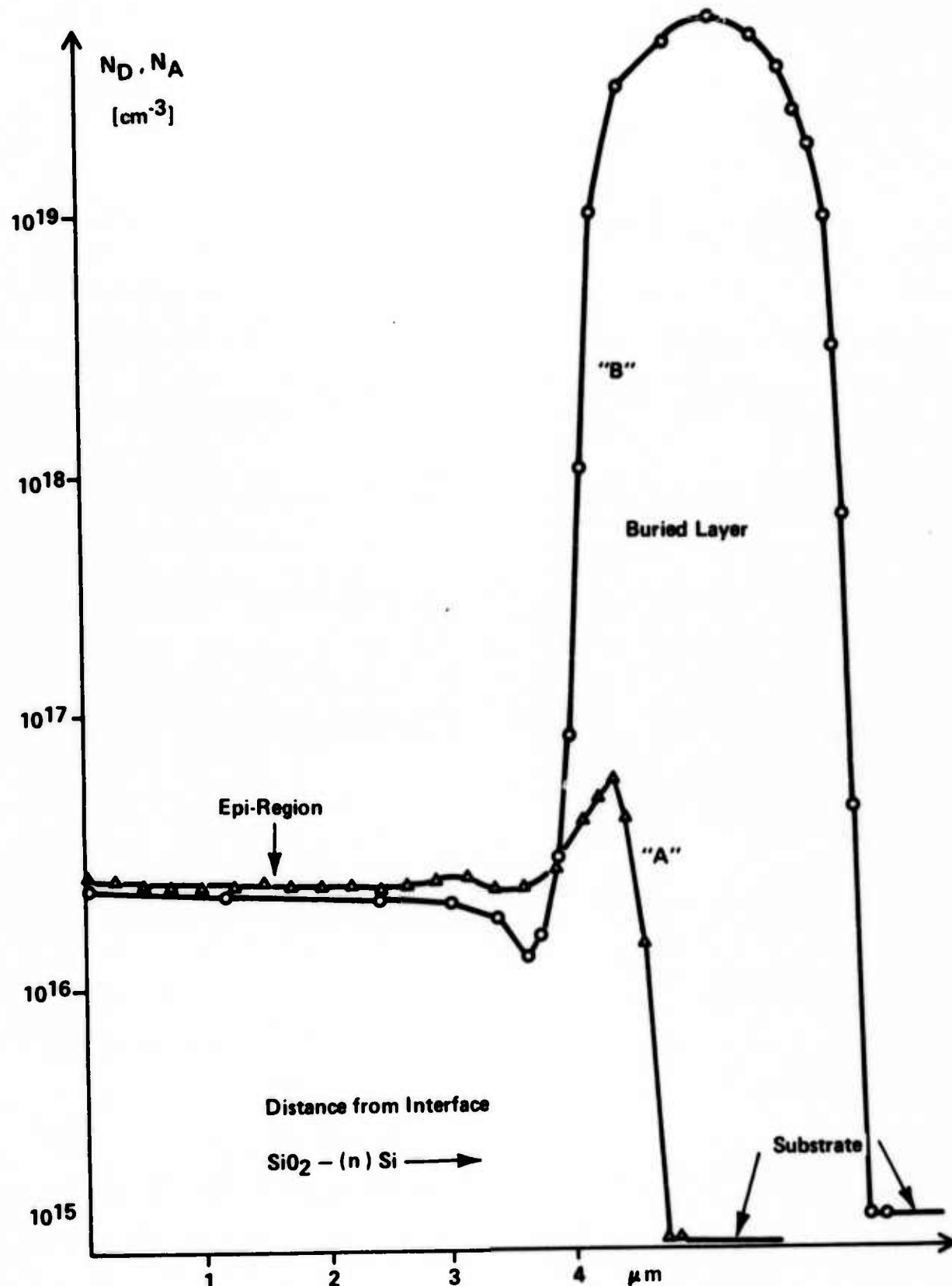


Fig. 2. Doping profiles underneath the dots A (triangles) and B (circles) in Fig. 1.

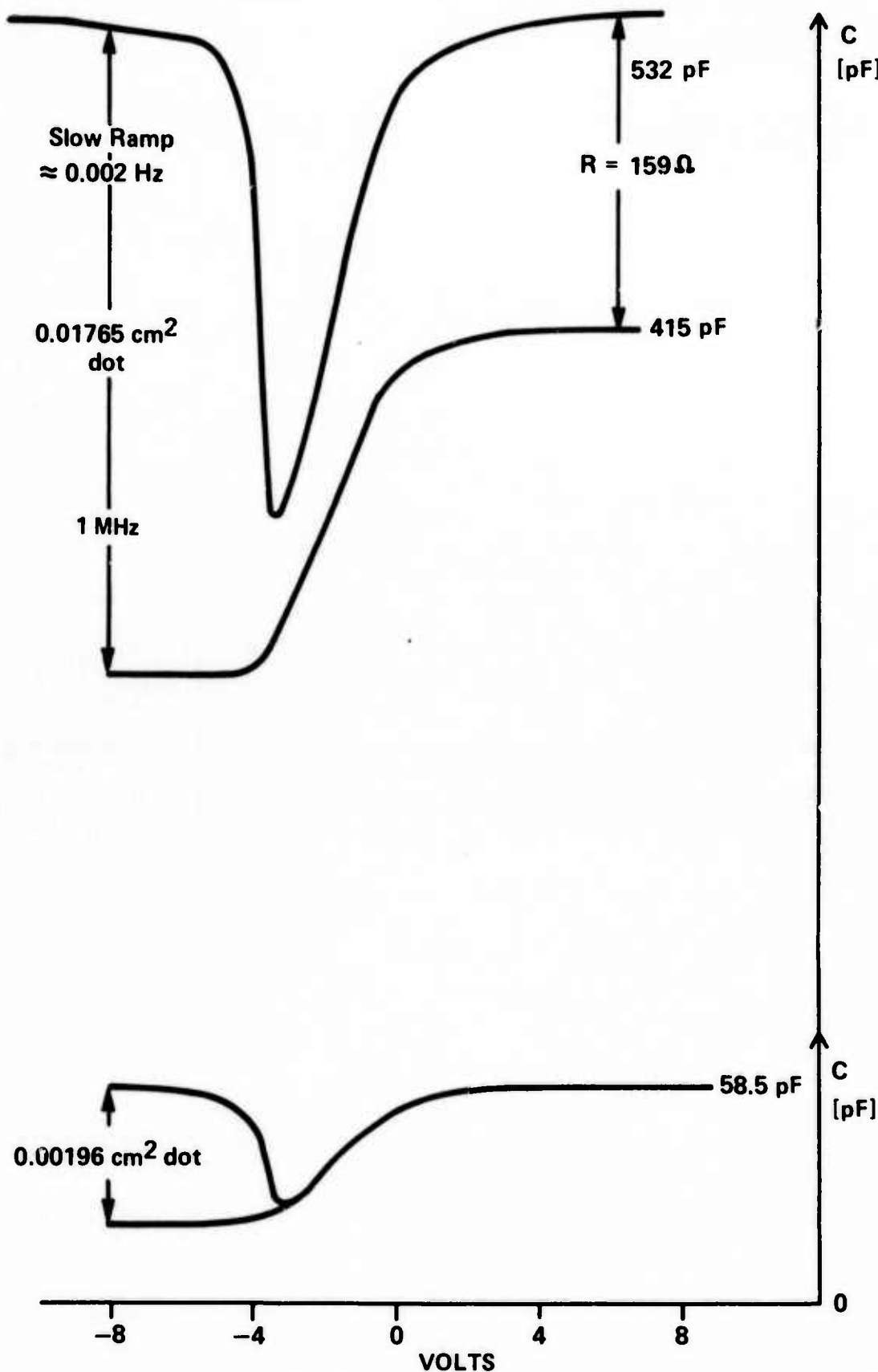


Fig. 3. C-V curves for two dots off the buried layer (A in Fig. 1).  
Note that for the smaller dot no dispersion is seen.

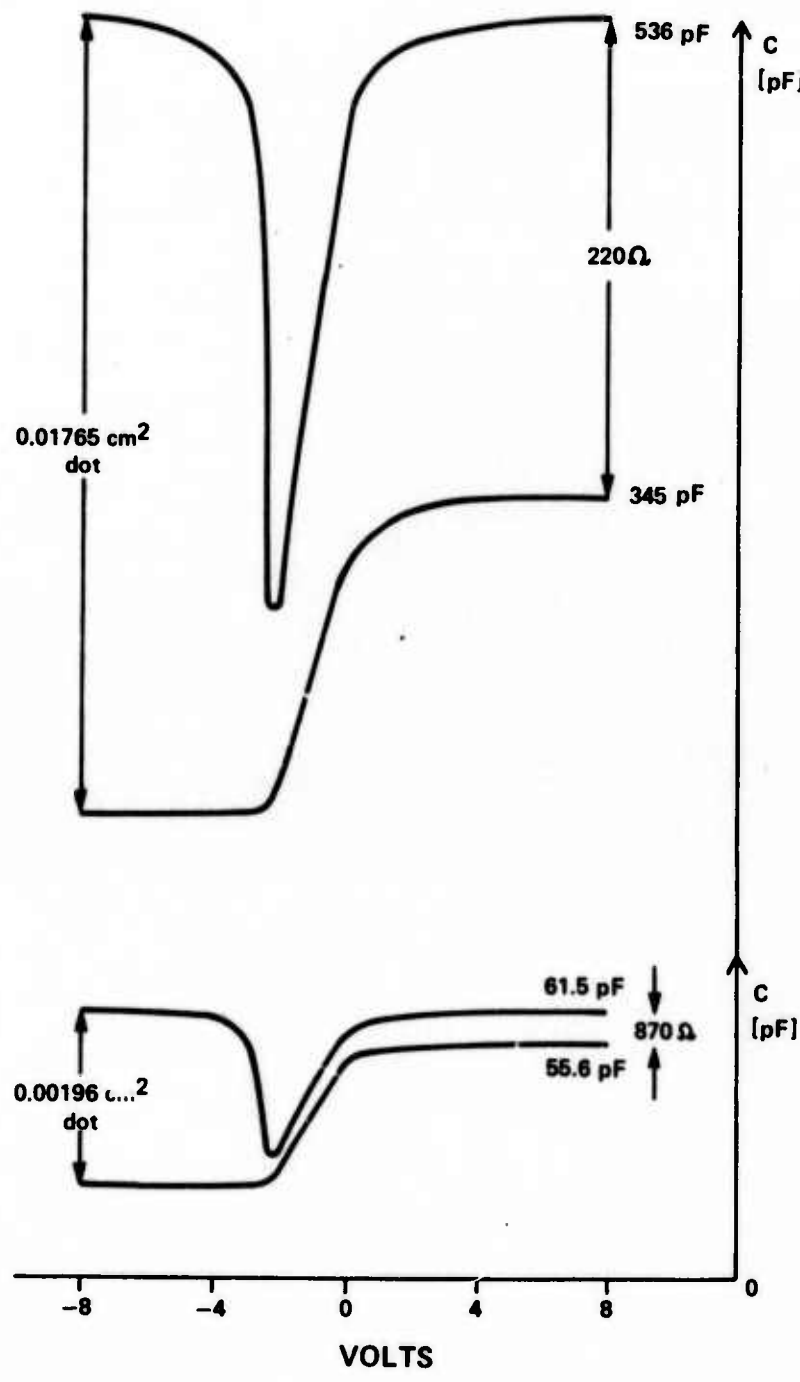


Fig. 4a. The same C-V curves as in Fig. 3 for a  $\langle 115 \rangle$  oriented substrate wafer. The epitaxial resistivity is three times larger than that in the samples characterized in Fig. 3.

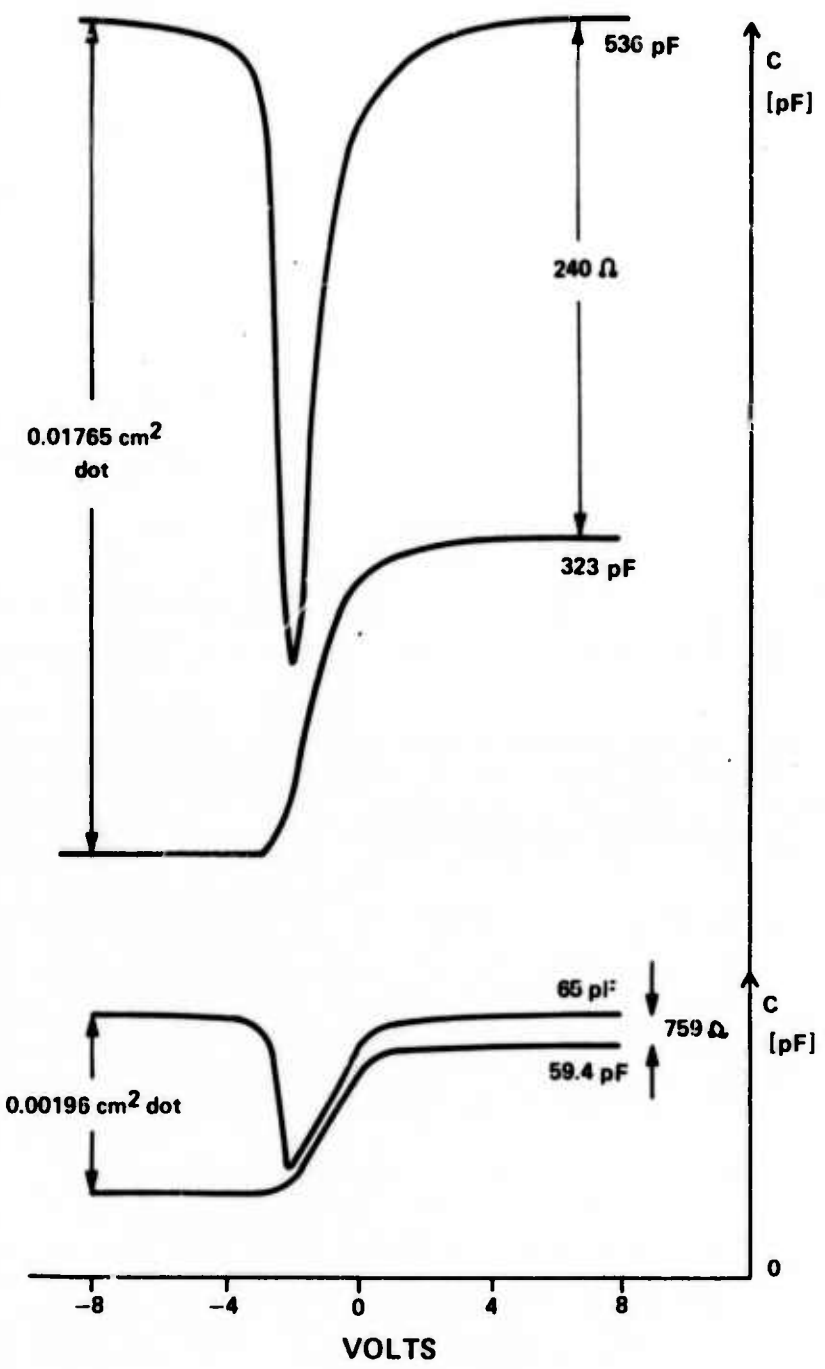


Fig. 4b. The same C-V curves as in Fig. 3 for a  $\langle 100 \rangle$  oriented substrate wafer. The epitaxial resistivity is three times larger than that in the samples characterized in Fig. 3.

value and the given wafer data, one obtains  $I_o \sim 10^{-9}$  A, and thus  $G_J \sim 4 \times 10^{-8} \exp(qv_J/kT)$  mhos. The capacitance  $C_J$  is  $\sim 20$  nf at 0 Volt and  $\omega C_J \sim 10^{-10}$  mhos for a frequency of  $2 \times 10^{-3}$  Hz. ( $I_o$  and  $C_J$  have been calculated by means of Shockley's equation  $I_o = qA (\frac{N_p}{N_D} \sqrt{\frac{D_p}{\tau_p}} + \frac{N_n}{N_A} \sqrt{\frac{D_n}{\tau_n}})$  and the depletion approximation  $C_J = \epsilon A (\frac{q}{2\epsilon v_D} \cdot \frac{N_D N_A}{N_D + N_A})^{1/2}$ .  $v_D$  is the diffusion potential. The other symbols have the usual meaning.) The ac admittance is resistance-controlled up to  $\sim 1$  Hz. Even in range  $f > 1$  Hz, there is no influence of the junction admittance, since  $\omega C_J \gg \omega C_{ox}$ . These considerations explain why a voltage-independent accumulation capacitance is measured over the usual frequency and bias range. The validity of the assumption on  $G(v_J)$ ,  $C(v_J)$ , and the numeric values are found in good agreement with  $C(v_J)$  and differentiated  $I(v_J)$  curves measured after oxide removal and ultrasonic cutting (e.g.,  $C_J = 35$  and  $40$  nf for dots cut at A and B, respectively).

The bulk resistance  $R_s$  of the substrate can be neglected as long as the resistivity is not too large. Experimentally, the upper limit was found to be approximately 50-100 ohm-cm and is theoretically given by the comparison of the  $RC_{ox}$  time constant with the measurement frequency of 1 MHz.

From the data given in Fig. 3 (i.e.:  $C_{ox} = 532$  pf,  $C_{HF}$  (acc.) = 415 pf), the lumped series resistance can be determined:

$$C_{HF} (\text{acc}) = C_{ox} / (1 + \omega^2 \tau^2) \quad [1]$$

$$\tau = RC_{ox} \quad [2]$$

This gives  $R = 159$  ohms. For the case of a buried layer underneath the dot, this value is reduced to  $R = 88$  ohms. (Note that in Fig. 2 the buried layer extends into the epitaxial layer due to outdiffusion.) When the dot area is reduced to  $0.00196 \text{ cm}^2$  and the capacitance to 58 pf, no dispersion is observed in accumulation up to 1 MHz. With the same values of  $R$ , one obtains now  $(\omega\tau)^2 = (2\pi \cdot 10^6 \cdot R \cdot C_{ox})^2 = 3.4 \times 10^{-3}$  and  $1 \times 10^{-3}$ , respectively;  $C_{ox}$  can be measured with 1 MHz.

Since the time constant of the surface states is usually observed in the kHz range,  $G(V)$  and  $G(\omega)$  measurements (2) are also feasible. (A  $G(V)$  and a  $G(\omega)$  curve is a plot of the total conductance  $G$  vs voltage or frequency at a fixed frequency or voltage respectively.) This is roughly checked by measuring  $G(V)$  in the kHz range. The typical peak due to surface states and its shift with frequency is observed.

From Fig. 4, one obtains  $R$  values of 220 ohms and 240 ohms for  $N_D = 5 \times 10^{15}$  and  $4.8 \times 10^{15} \text{ cm}^{-3}$ , respectively.

## SPREADING RESISTANCE VS DOT DIAMETER

For frequencies  $\omega \leq 1/RC_{ox}$ , the equipotential lines of the structure are schematically drawn in Fig. 5a. Therefore, one can assume a disk-like volume representing the epitaxial layer, in which the current flows (Fig. 5b). The voltage  $v_o$  is applied at the inner area  $2\pi r_o^2 d_{epi}$ ,  $d_{epi}$  being the epitaxial layer thickness; the outer area at  $r_1$  is grounded. A voltage  $dv$  drops across a volume increment  $2\pi r^2 dr \cdot d_{epi}$ :

$$dv = -i_o dr$$

( $i_o$  is the current caused by  $v_o$ ).

$dR$  is defined by

$$dR = \rho \cdot dr / A(r) = \rho \cdot dr / (2\pi r^2 d_{epi})$$

$$dv = -i_o \cdot \rho \cdot dr / (2\pi r^2 d_{epi})$$

$$v = - (i_o \cdot \rho / 2\pi d_{epi}) \ln (r/r_1).$$

Since  $v(r_o) = v_o$ :

$$(v_o / i_o) = R = - (\rho / 2 d_{epi}) \ln (r_o / r_1) \quad [3]$$

As a result, one obtains an increase of the spreading resistance for smaller dot diameters. For the epitaxial wafers of Figs. 2 and 3, we are not able to observe this change, first because the spreading resistance is too small, second, because the existence of the junction and oxide capacitance heavily interferes with the assumption of a simple radial current. For the SOS wafers shown here, however, the effect is clearly visible. For an oxide of 1300 Å, and an  $\sim 10\text{-}\mu\text{m}$ -thick epitaxial layer of 1 ohm-cm, one obtains  $R = 500, 1380$ , and  $\sim 2450$  ohms for dots of  $0.01765, 0.00196$ , and  $0.00049 \text{ cm}^2$ ,

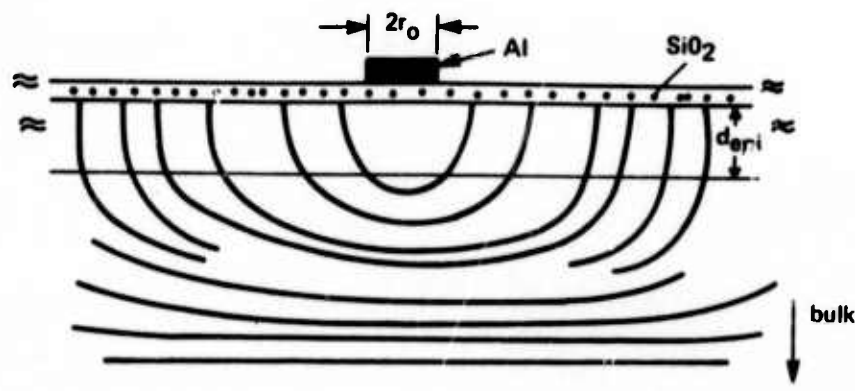


Fig. 5a. Equipotential lines for frequencies  $\ll 1$  MHz. The current flow in the epitaxial layer is practically radial.

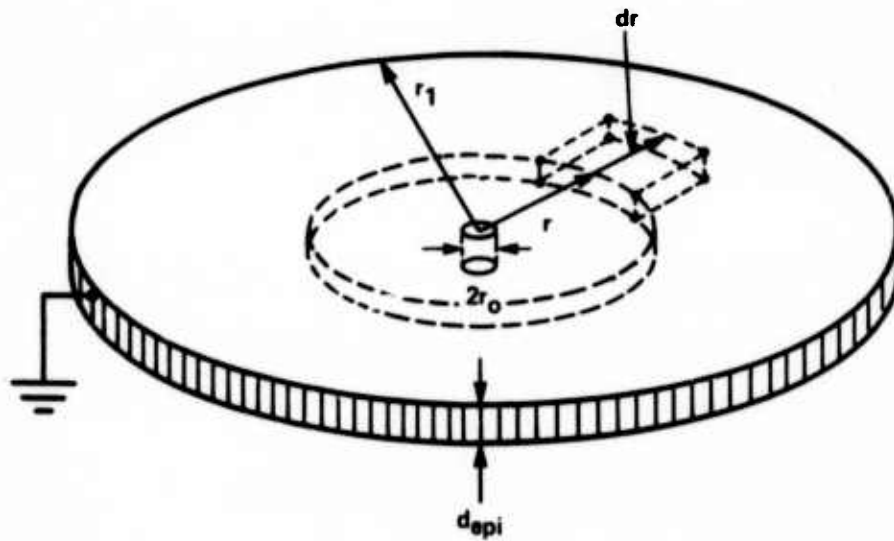


Fig. 5b. The epitaxial layer in a simplified disk-like geometry.  
For  $r < r_o$ , the potential is assumed to be constant ( $= v_o$ ).

respectively. Since, for these structures, contact with the backside is made by overlapping Al at the edge of the wafer, the spreading resistance is measured without distortion by the junction capacitance. Though we do not observe an  $R \propto (-\ln r_0)$  dependence but, rather, an  $R \propto 1/r_0$  one, the model qualitatively describes the behavior of the spreading resistance.

#### RANGE OF QUASI MOS CAPACITANCE TECHNIQUE

In the preceding sections, we have shown that the contribution of the junction impedance can be neglected, if appropriate values for the resistivities, oxide thickness, dot diameter, etc., are selected. In the following, we give approximate ranges for those parameters. Within these ranges, the junction impedance is small compared with the interface, oxide, and layer impedance.

For a 5- $\mu\text{m}$  layer of  $\rho \sim 0.3 \text{ ohm}\cdot\text{cm}$  resistivity and  $1200 \text{ \AA SiO}_2$ , a dot of  $d \leq 0.5\text{-mm}$  diameter should be used. The substrate might have  $\rho \leq 20 \text{ ohm}\cdot\text{cm}$ . For other oxide thicknesses  $d_{\text{ox}}$ ,  $d$  can be chosen to be  $d = \frac{0.5}{1200} d_{\text{ox}}$ . For higher layer resistivities, the layer thickness should be increased according to the resistivity ratio. For epitaxial  $\rho$  values  $\geq 15 \text{ ohm}\cdot\text{cm}$ , care must be taken that the condition  $C_{\text{ox}} \ll C_J$  is still valid, e.g., by increasing the wafer area. For the insulator-silicon structure, with an oxide thickness of  $1300 \text{ \AA}$  and a layer of

$\sim 10 \mu\text{m}$  and  $N_D, N_A \sim 1-2 \times 10^{16} \text{ cm}^{-3}$ , we consider a dot of 0.25-mm diameter as appropriate. The same changes in dot diameter and epitaxial layer thickness should be done for a variation in oxide thickness and layer resistivity. The diameter of the wafer should be at least 1-1/4 inches. Since these values refer to the oxide capacitance ( $\tau = RC_{ox}$ ) and the lifetime measurements are carried out with the inversion and deep depletion capacitance (8), the accuracy increases by  $(C_{ox}/C_f)^2$ . (Cf. Eq. [1].)

#### COMPARISON WITH OTHER TECHNIQUES

Finally, this technique should be compared with some alternatives, namely, the MOS emitter device and the buried-layer SOS structure, described, for example, in Refs. (9) and (10). Though some restricting conditions are implied in our technique, such as dot diameter, epitaxial layer thickness, etc., its advantages are greater versatility and measurement without distortion of a conduction layer. For example, the technique of Jones and Barber (9) is restricted to lifetimes, whereas a buried conduction layer (10) might cause out-diffusion and thus a reduction of lifetimes even in the epitaxial bulk.

Measurements using a guard ring as a counterelectrode were made. The substrate was at the same potential as the guard ring. The equivalent network consists of the oxide and space charge capacitance,  $C_{ox}$  and  $C_{sc}$ , respectively, of the dot

in series with the oxide capacitance  $C_{oxR}$ , the space charge capacitance  $C_{scR}$  of the ring, and the spreading resistance of the layer. The network is shunted by the coupling capacitance  $C_c$  between the dot and the ring. (We neglect here the shunt to the substrate, because this has been discussed above.) The condition  $C_{ox} \ll \frac{C_{oxR} \cdot C_{scR}}{C_{oxR} + C_{scR}}$  can be fulfilled by the appropriate choice of the ring area. The condition  $C_c \ll \frac{C_{ox} \cdot C_{sc}}{C_{ox} + C_{sc}}$  is always valid since oxide thicknesses of 500...5000 Å are used. For a dot diameter of 60 mils, an oxide of 1000 Å, and a spacing of 150 µm, one obtains  $C_c = 10^{-4}$  pf. Thus dispersion-free C-V curves are feasible. This was confirmed by the experiment. However, a disadvantage is encountered: with the present state of the art, photoresist deteriorates the oxide and silicon properties, especially the lifetimes and the oxide stability. We observed reductions in lifetimes from 500 µsec to 0.1 µsec and flatband shifts. (The lifetime data of the paper were obtained by the technique given in Ref. 8.)

#### RESULTS AND DISCUSSION

The results of the measurements can be summarized as follows: Flatband voltages and surface-state densities are found in the usual ranges of  $\sim -1V$  and  $\leq 1.4 \times 10^{10} \text{ eV}^{-1} \text{ cm}^{-2}$ , respectively.

Since the peak of the G-V curves is found at depletion surface potentials for frequencies in the kHz range, the capture cross section can be expected to be  $10^{-13}$  to  $10^{-15} \text{ cm}^2$ . No deviation compared with "normal" MOS structures can be seen. Lifetimes are measured to be 1  $\mu\text{sec}$  in the epitaxial wafers,  $10^{-3} \mu\text{sec}$  in the n-SOS wafers, and 0.1  $\mu\text{sec}$  in the p-SOS wafers.

The SOS low-frequency curves for wafers of layer thicknesses between 1 and 10  $\mu\text{m}$  do not show any trace of a donor or an acceptor level (Fig. 6). This is in contradiction to earlier reports (11, 12), where an acceptor and a donor level at  $E_c - E_A = 0.25 \text{ eV}$  and  $E_D - E_v = 0.30 \text{ eV}$  were published. This might be attributed to different measurement techniques. The densities of the levels are reported to be  $10^{17}$  to  $10^{18} \text{ cm}^{-3}$ . A good resolution for surface states (or bulk impurities seen as surface states) for the slow ramp technique is  $10^{11} \text{ cm}^{-2}$ . If this value is divided by an effective distribution width of 10 to 100  $\text{\AA}$ , one obtains bulk concentrations of  $10^{17}$  to  $10^{18} \text{ cm}^{-3}$ . The slow ramp technique, however, measures states localized at the surface, whereas the techniques used in Refs. (11) and (12) cover the total depth of the film. Thus, it might be concluded that the reported levels are located near the Si-Al<sub>2</sub>O<sub>3</sub> interface.

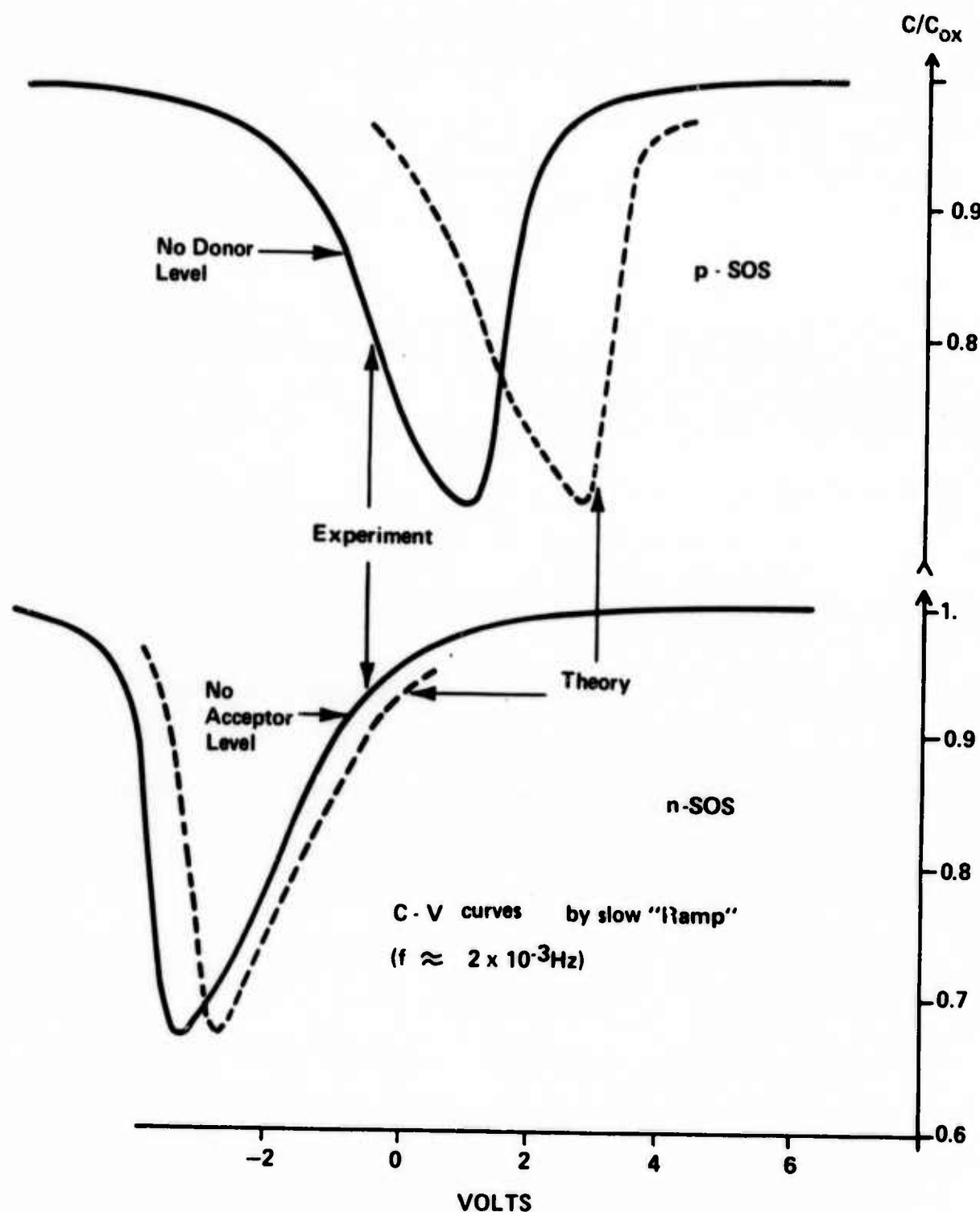


Fig. 6. Enlarged portion of the low frequency C-V curve of a p- and n- SOS wafer. No indication of a deep lying level is visible. For comparison, the ideal low frequency curves are shown too.

Another possible explanation is the fact that one deals with extremely deep levels. Their time constant is controlled by the surface potential  $u_s$ :

$$\tau_p = (\sigma \cdot v_{th} \cdot N_A)^{-1} \exp(-u_s)$$

Since the levels are defined to be either acceptor or donor levels, they exchange carriers only with the valence or conductance band, respectively. With the given data and an assumption of a capture cross section  $\sigma = 10^{-15} \text{ cm}^2$  and a thermal velocity  $v_{th} = 10^7 \text{ cm/sec}$ , one obtains for the hole dispersion time constant in the n-type wafer  $\tau_p = 2 \times 10^2 \text{ sec}$ . This value is comparable to our measurement frequency of  $2 \times 10^{-3} \text{ Hz}$ . Capture cross sections of  $10^{-15} \text{ cm}^2$  have been measured (13); in this case, however, higher values are more likely, and the first explanation should be preferred.

#### SUMMARY AND CONCLUSIONS

The measurement of the admittance of an MOS structure over a p-n junction or on SOS devices is discussed. It is shown that by appropriate choice of the wafer data, the contribution of the junction to the total admittance can be neglected and lifetime measurement can be carried out.

No deep levels can be seen for the SOS system.

## REFERENCES

1. R. Castagne, C. R. Acad. Sc. (Paris), 267, Serie B,  
866 (1968).
2. E. H. Nicollian and A. Goetzberger, Bell System Tech. J.,  
46, 1055 (1967).
3. D. R. Kerr, Int. Conf. on Properties and Use of MIS  
Structures, J. Borel, Editor, CNRS-LETI, Grenoble, 303 (1969).
4. W. R. Fahrner and A. Goetzberger, Appl. Phys. Lett.,  
21, 329 (1972).
5. M. Zerbst, Z. Angew. Phys., 22, 30 (1966).
6. P. Rai-Choudhury and D. K. Schroder, J. Electrochem. Society,  
119, 1580 (1972).
7. Technical Report No. 4.
8. W. R. Fahrner and C. P. Schneider, ESSDERC, Nottingham,  
England (1974).
9. J. E. Jones and H. D. Barber, IInd Int. Symp. on Silicon  
Materials Science and Technology, March 13-18, Chicago,  
561 (1973).
10. D. K. Schroder and P. Rai-Choudhury, Appl. Phys. Lett.,  
22, 455 (1973).
11. F. P. Heiman, ibid., 11, 132 (1967).
12. D. J. Dumin, Solid-State Electron., 13, 415 (1970).
13. W. Fahrner and A. Goetzberger, Appl. Phys. Lett., 17  
16 (1970).